CHALMERS

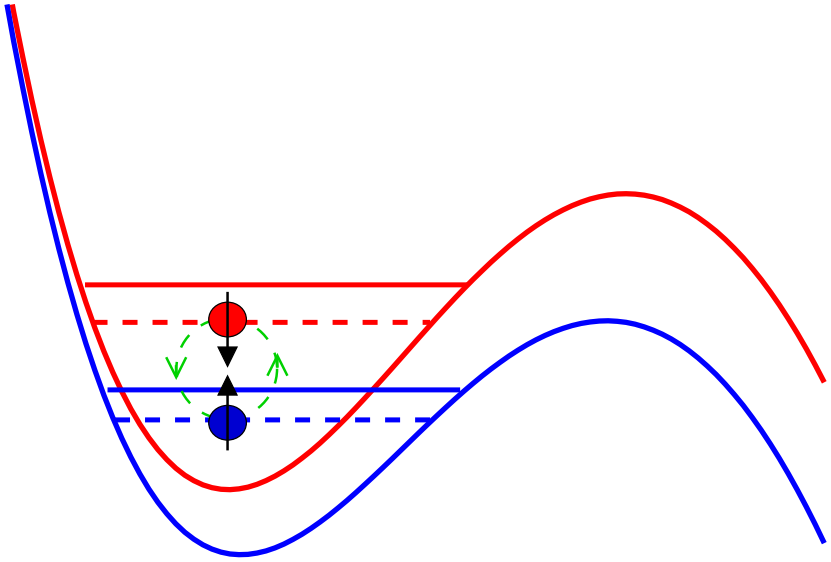

Tunneling Theory for Few-Body Systems in One-Dimensional Traps

Thesis for the Degree of Master of Science

Rikard Lundmark

Department of Fundamental Physics
Chalmers University of Technology
Gothenburg, Sweden 2014

Thesis for the Degree of Master of Science

Tunneling Theory for Few-Body Systems in One-Dimensional Traps

Rikard Lundmark

Department of Fundamental Physics
Chalmers University of Technology
Gothenburg, Sweden 2014

Tunneling Theory for Few-Body Systems in One-Dimensional Traps
Rikard Lundmark

Department of Fundamental Physics

Supervisor: Christian Forssen, Department of Fundamental Physics
Examiner: Gabriele Feretti, Department of Fundamental Physics

Department of Fundamental Physics
Chalmers University of Technology
SE-412 96 Göteborg
Sweden
+46 (31) 772 1000

Printed by Chalmers reproservice
Göteborg, Sweden 2014

Abstract

In recent experiments, carried out at the University of Heidelberg, tunneling rates of ultracold distinguishable fermions out of an optomagnetical trap have been measured. The fermions interact by a tunable short-ranged interaction, and the trap is asymmetric making the trapped quantum system effectively one-dimensional.

In this thesis, a method for calculating the energy levels and tunneling rates of one and two interacting particles out of a very general one-dimensional potential well is devised. The method is based on expanding the Schrödinger equation of the system in a complex-momentum basis. This is done utilizing the so-called Berggren completeness relation. Ultimately, the basis expansion leads to a complex symmetric non-Hermitian eigenvalue problem for a large, dense matrix.

The general method is applied to a system of trapped, ultracold fermionic atoms in a setup that closely resembles the Heidelberg experiments. The short-ranged interaction is modeled as a point-interaction, and the trap potential is regularized at large distances from the interesting region.

The obtained energies and decay rates are contrasted to results obtained using the Wentzel–Kramers–Brillouin (WKB) approximation. Notable differences can be observed, and these may be due to insufficiency of the WKB approximation to accurately describe the system in question.

Acknowledgements

I would like to thank all the people whose help and support has made this project possible.

First and foremost, I would like to thank my supervisors, Christian Forssén and Jimmy Rotureau, for lots of invaluable discussions, support and good advice regarding all aspects of the project.

I would also like to mention the members of the Subatomic Physics Group that were not directly involved in this project. An important contribution was made by Håkan Johansson, who was available for technical support seemingly around the clock. Also, I would like to mention Boris Carlsson, for technical support and for his useful program to distribute calculations over several computers.

Rikard Lundmark, Gothenburg, April 2014

Contents

Chapter 1

Introduction

For ultracold[1] atoms, quantum mechanical properties become important. Studying such atoms may therefore give insights into various highly interesting phenomena. Of particular interest for this work are interacting, distinguishable fermions in one dimension. For a weak[2] interaction between such fermions, they will pair up in a way resembling the BCS theory of superconductivity [1].

If instead the inter-fermion interaction is strongly repulsive, the fermions will repel each other and behave like identical fermions, which obey the Pauli principle. This phenomena is known as *fermionization*. For a strong attractive interaction between the fermions, the energy spectrum will be similar to the strongly repulsive case, with a notable difference being an additional state at the lower end of the spectrum. Using an interaction with a variable strength, it is possible to study the crossover between these different regimes of interaction strengths. This includes studying the crossover between strongly attractive and strongly repulsive attraction when the attraction strength passes through infinity [1, 2, 3].

In recent experiments at the University of Heidelberg [2, 3], a system consisting of a few ultracold fermions in an asymmetric quasi one-dimensional trap is studied. In particular, tunneling of the fermions out of the trap is measured. The fermions interact with a short-ranged inter-particle force, and the strength of the force is tunable by a so-called Feshbach resonance. The short-range property of the inter-particle force allows it to be described by a contact interaction. Using only a few fermions creates an opportunity to understand how many-body properties of strongly interacting fermionic systems arise from the more fundamental few-body properties. By adding more and more fermions, it is possible to study the transition from few-body systems to many-body systems [1].

[1] Atoms cooled to temperatures very close to the absolute zero, 0 K.

[2] Weak is here defined as a small interaction energy compared to the spacing between the energy levels of non-interacting particles.

Theoretical modelling of systems like the Heidelberg one has already been attempted using different methods, such as the Wentzel–Kramers–Brillouin approximation [4, 5]. This work takes a different approach by using a basis expansion of a many-particle wavefunction to solve the problem numerically. This method has previously been applied to theoretical nuclear physics, where it can used to compute energies and decay rates for bound and resonant states in nuclear many-body systems [6, 7].

1.1 Purpose and Scope

The purpose of this Master's thesis project can loosely be divided into two parts:

1. Develop a method for finding energies and tunneling rates of bound and resonant one- and two-particle states in a one-dimensional potential well, under certain conditions[3].

2. Apply this method to a system resembling the quantum system studied experimentally by the Heidelberg group, and compare the results to the experimental ones and to other theoretical results.

1.2 Outline

The thesis is structured as follows. First some units and conventions used in the thesis are introduced, which is done in Section 1.3. After that follows a brief overview of the experimental procedures (Chapter 2) for the main experiment that the results of this thesis is compared to. This leads up to a description of the relevant 1D quantum system. Thereafter, in Chapter 3, a theoretical background with derivation of relevant equations is presented.

The theory is followed by details on how it was implemented in calculations (Chapter 4). After that, some benchmarking is presented in Chapter 5, where the results obtained by the basis expansion method are compared to results obtained by other methods. Results of the comparison with the Heidelberg system are presented and discussed in Chapter 6. The results are also compared to experimental data and other theoretical papers.

Finally, the thesis is concluded by Chapter 7 where the future outlook of the subject is studied.

A glossary, describing words and concepts occurring in the thesis, can be found in Chapter 7. Some further additional details on certain specific topics can be found in the appendices.

[3]The conditions include requiring the potential to be zero outside some finite region, as well as assuming a specific form of the inter-particle interaction. These conditions will be further elaborated in Chapter 3–4.

Additional documentation and source code used in this project can be downloaded from `rikardlundmark.com/tunnelingtheory`.

1.3 Units and Conventions

In this thesis, predominantly non-SI units are used. The dominating set of units is *molecular units*, which is assumed if nothing else is stated. In some cases, mainly when comparing with other experimental and theoretical results, harmonic oscillator units are used.

Quantity	**Molecular Units**		**HO Units**
	Value	**SI Value**	**Value**
Length L	$1\,\mu$m	$10^{-6}\,$m	$\sqrt{\hbar/(m\omega)}$
Mass M	$1\,\Omega$	$1.782\,661\,8\cdot10^{-30}\,$kg	m
Time T	$1\,\mu$s	$10^{-6}\,$s	$1/\omega$
Energy E	$1\,\mu\mathrm{K}\cdot\mathrm{k_B}$	$1.380\,648\,8\cdot10^{-29}\,$J	$\hbar\omega$

Table 1.1. *Definitions of quantities in molecular units. The temperature unit may be taken to be Kelvin. For the harmonic oscillator units, ω is an angular frequency used to characterize the system.*

1.3.1 Molecular Units

The definitions of some quantities in molecular units, expressed in SI units, can be found in Table 1.1. They are obtained by choosing the quantities, given in the first column, to be expressed in the units of the SI value, given in the second column of the table. The mass unit, denoted by Ω, is uniquely defined from the other three units in the table by the relationship

$$[E] = [M]\,[L]^2\,[T]^{-2}$$

In this thesis, there are two main quantities that needs to be expressed in these units. One is the Planck constant, $\hbar \approx 7.638\,233\,0\,\mu\mathrm{K}\cdot\mathrm{k_B}\cdot\mu$s. The other one is the mass of ^{6}Li. In SI units the latter is $6.015\,122\,8$u, which becomes $723.453\,025\,1\Omega$ in the molecular units.

These values are used in the majority of all numerical calculations in this thesis. Another set of units would of course have produced the same final result. The reason for choosing molecular units is that the available experimental data, most importantly the shape of the potential, are given in these units, which simplifies a comparison between this thesis and the work of others.

1.3.2 Harmonic Oscillator Units

Harmonic oscillator units are obtained by expressing energy and length using a reference frequency ω. The relation between these units and molecular units is described in Table 1.1.

1.3.3 Notation and Assumptions

Standard Dirac notation is used throughout the thesis. The inner product between two states will be redefined in Section 3.3.1 to an inner product without conjugation in order to make non-Hermitian quantum mechanics possible.

This thesis exclusively deals with non-relativistic quantum mechanics. Since the system under consideration consists of ultracold atoms, the energy is low which motivates this approximation.

Chapter 2

Experimental Background

Experiments with strongly interacting ultracold atoms have been carried out at the University of Heidelberg [1, 2, 3]. Although the method developed in this thesis applies to a general one-dimensional quantum system, a main objective is to make comparisons with results from the Heidelberg experiments. Therefore, a brief description of the quantum system that these experiments probe is given in this Chapter. An analytic expression for the trapping potential of the quantum system is introduced, and the different channels for two atoms tunneling out of the trap are described.

2.1 The Heidelberg Quantum System

The quantum system under consideration consists of ultracold ^{6}Li atoms inside an optomagnetical trap, out of which the particles may tunnel in essentially one direction. Since ^{6}Li has spin 1/2, these atoms will act as fermions. ^{6}Li has different hyperfine states, and in this thesis the two lowest (in terms of energy) will be considered. These are denoted by $|\uparrow\rangle$ and $|\downarrow\rangle$ to distinguish between them. In a magnetic field the energy of the states will differ, making them distinguishable.

In this thesis, both the case of one and the case of two particles inside the trap are considered. With one particle, the state is of no other practical importance than determining the potential shape, since particles in different states may experience slightly different potentials.

If two particles are present in the trap, interaction between them occurs if one particle is in state $|\uparrow\rangle$ and one is in state $|\downarrow\rangle$. The inter-particle interaction can be tuned by means of a so-called Feshbach resonance. Some more details on this topic can be found in Appendix C. Essentially, it means that it is possible to experimentally alter the strength of the inter-particle interaction by changing the magnetic field strength in the experiment.

The interaction between the particles is short-ranged, and therefore modeled as a point interaction. This means that it can be written in a simple

form as a so-called coupling coefficient g times some delta functions, expressed by Equation (3.17). The value of the coupling coefficient g is the quantity controlled by the Feshbach resonance.

It is then also clear why there is no interaction if both particles are in state $|\uparrow\rangle$ or $|\downarrow\rangle$. Due to the Pauli principle the joint wavefunction must be antisymmetric, and a contact interaction will then give zero contribution.

2.2 Trapping Potential

The optomagnetical trap potential is "cigar-shaped" [1] close to its bottom, as illustrated by Figure 2.1. In its full three-dimensional form, it is given by

$$V(x, y, z) = V_x(x) + V_y(y) + V_z(z) \tag{2.1}$$

where $V_x(x)$ and $V_y(y)$, denoted as the perpendicular components, are given by

$$V_s(s) = pV_{0r}(s)\left(1 - e^{-\frac{2s^2}{w_{0s}^2}}\right) \tag{2.2}$$

with $s \in \{x, y\}$ and the parameters are as in Table 2.1. The part of the magnetic field parallel to the z-axis is given by

$$V(z) = pV_0\left(1 - \frac{1}{1 + \left(\frac{z}{z_r}\right)^2}\right) - c_{B|\text{state}\rangle}\mu_m B' z \tag{2.3}$$

with parameters given by Table 2.2. It should be noted that the trap parameters are obtained from a combination of experimental results and WKB theory [1, 2, 3].

The state dependence of the potential, mentioned above, is contained in the factor $c_{B|\text{state}\rangle}$. This one-dimensional potential is illustrated in Figure 2.2 for some choices of the constituting parameters. The second term in (2.3) is due to an applied magnetic field gradient B' with the purpose of causing the trap asymmetry, with the intention of making unidirectional tunneling possible.

The aspect ratio[1] of the perpendicular and parallel parts of the trapping potential is 1:10 [1, p. 149]. This motivates the 1D simplification on which this thesis is based. The particle is seen as fixed in the x- and y-directions, and only the z-direction is considered.

[1] Defined as the ratio between the angular frequencies in the harmonic approximation of the potential.

Parameter	Value	Designation
V_{0r}	$4.120\mu\mathrm{K} \cdot \mathrm{k_B}$	Potential depth.
w_{0x}	$1.637\mu\mathrm{m}$	Waist depth.
w_{0y}	$1.516\mu\mathrm{m}$	Waist depth.

Table 2.1. *Parameters for the potential in the perpendicular direction, as given by Equation* (2.3)*. In the equation, s is either the x or the y-coordinate. p is a parameter also occurring in Equation* (2.3)*, which determines the potential depth.*

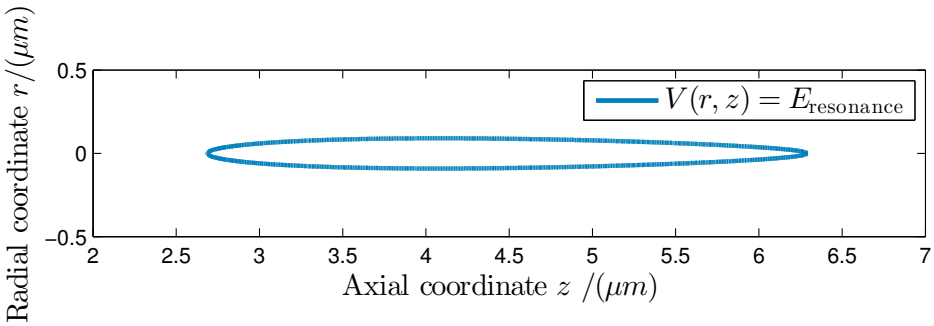

Figure 2.1. *Cross section of equipotential surface for the lowest resonant state in the trapping potential* (2.1)*. The radial coordinate r is perpendicular to the z-axis.*

Parameter	Value	Designation
V_{0r}	$3.326\mu\mathrm{K} \cdot \mathrm{k_B}$	Potential depth.
z_R	$9.975\mu\mathrm{m}^2$	Rayleigh range of trapping beam.
μ_B	$6.717\,138\,8 \cdot 10^5\,\mu\mathrm{K} \cdot \mathrm{k_B/T}$	Bohr magneton.
B'	$18.92 \cdot 10^{-8}\,\mathrm{T}/\mu\mathrm{m}$	Magnetic field gradient.
$c_{B\|\mathrm{state}\rangle}$	≈ 1	See caption.

Table 2.2. *Parameters for the potential in Equation* (2.3)*. In the equation, z is the position along the main axis, given in μm, and p is a dimensionless parameter with a value depending on the number of particles in the trap. For two particles, $p = 0.63496$ [3]. $c_{B\|state\rangle}$ is a parameter approximately equal to one, and its value depends on both the interaction strength and the state of the particle.*

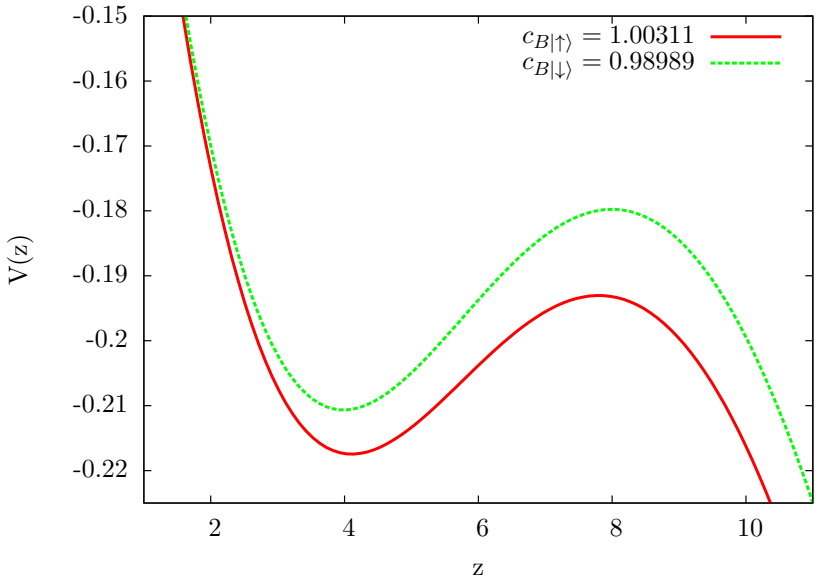

Figure 2.2. *The trapping part of the potential* (2.3) *for two particles in different hyperfine states in the same magnetic field, as described by [3].*

2.3 Tunneling out of the Trap

An important observable measured in the Heidelberg experiment is the tunneling rate of the fermions out of the trap. A single particle in the potential may tunnel out through the barrier to be detected. For two interacting particles, the tunneling process can be slightly more complicated. Tunneling can then happen as a combination of two limiting cases. Either on particle tunnels out first, which can alter the energy of the other particle. The other particle can subsequently tunnel out after that. Tunneling could also happen by both interacting particles tunneling out together, so-called pair tunneling. The different tunneling channels are illustrated in Figure 2.3. In practice, both channels contribute.

Using the basis expansion method, which will be introduced in the next section, it will be possible to calculate both the single-particle tunneling rate and the total tunneling rate of two particles out of the trap.

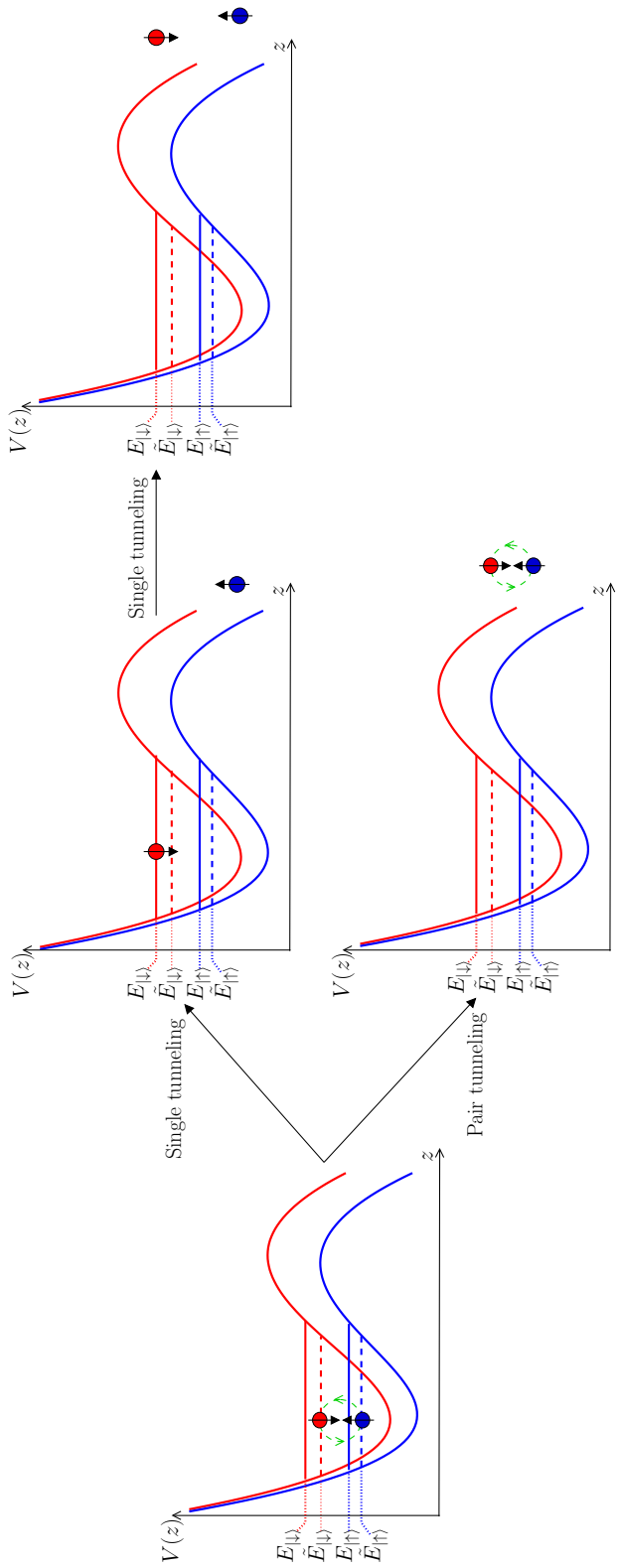

Figure 2.3. *Illustration of two interacting fermions in different states in a trap, and their tunneling channels. The unperturbed energy levels of the particles are indicated with solid lines. When the particles interact, the energy levels change. This is illustrated in the figure for an attractive interaction, which lowers the total energy of the particles. The assignment of this energy difference to the particles is arbitrary, and the dashed lines indicating the new energy levels are thus for illustrative purposes only. As can be seen in the figure, the interacting particles can tunnel through two different channels: either as a pair, or in a sequence. When the particles tunnel sequentially, the tunneling particle will necessarily carry the interaction energy since the remaining particle must have enough energy to be in its ground state. The sequential tunneling illustrated in the figure could also happen in the opposite order, so that the $|\downarrow\rangle$ particle tunnels first. By the methods employed in this thesis, the total tunneling rate for all tunneling channels will be calculable, as will become clear in the following sections.*

Chapter 3

Theory

The main goal of this chapter is to derive methods for expanding the Schrödinger equation in a complex momentum basis. This basis expansion will then lead to an eigenvalue problem, from which the energies and tunneling rates of particles out of a potential can be obtained. First, an introduction to complex energy and momenta is given, and the important Berggren completeness relation is stated. Thereafter, a motivating example, a piecewise constant potential that gives rise to resonances, is given. Following that, the basis expansion is introduced, and a suitable momentum space basis is chosen. A one-particle basis expansion is performed in detail using this basis. We then introduce a harmonic oscillator basis, and use it to compute the matrix elements of the inter-particle interaction for two particles. These matrix elements are then used to construct a two-particle basis expansion. Finally, some theory used for verification and approximation procedures is briefly mentioned.

3.1 Introduction

By the postulates of quantum mechanics, a physical system is associated with a Hilbert space $\mathcal{H}$ together with an inner product. The state of the system is described by a one-dimensional subspace $\{|\psi\rangle\} \in \mathcal{H}$.

A physical observable is described by a Hermitian operator acting on the Hilbert space. In the Schrödinger picture, operators are taken as constant in time while states are allowed to change under time evolution. The dynamics of a system is then described by the Schrödinger equation

$$i\hbar\frac{\partial}{\partial t}|\psi\rangle = H|\psi\rangle \tag{3.1}$$

where H is the Hamiltonian (energy operator) of the system.

For a particle of mass m in one dimension, the time-independent Hamil-

ton operator may be expressed in the position coordinate x as

$$H = -\frac{\hbar^2}{2m}\frac{\partial^2}{\partial x^2} + V(x)$$

where $\hbar$ is the Planck constant and $V(x)$ is the potential that the particle experiences.

For a *stationary state*[1] $|\psi_E\rangle$ of H with energy E the temporal and spatial dependence can be separated, $\langle x,t|\psi_E\rangle \equiv \psi_E(x,t) = \eta_E(t)\chi_E(x)$. Substituting this into the Schrödinger equation gives the temporal part as $\eta_E(t) = e^{-iEt/\hbar}$. Thus the Schrödinger equation for an eigenstate reduces to the so-called time-independent Schrödinger equation

$$H\,|\chi_E\rangle = E\,|\chi_E\rangle \tag{3.2}$$

It can be shown that any solution $|\psi\rangle$ of the Schrödinger equation can be written as a linear combination of the full set of eigenstates $\{|\psi_E\rangle\}$, and this set therefore constitute a complete basis, the *energy spectrum* for the Hilbert space. This means that we can write [8, p. 19, p. 41]

$$\sum_{n\in\text{bound states}} |\psi_{E_n}\rangle\langle\psi_{E_n}| + \int_0^\infty \mathrm{d}k\,|\psi_{E_k}\rangle\langle\psi_{E_k}| = \mathbb{1} \tag{3.3}$$

where $|\psi_{E_n}\rangle$ are bound states and $|\psi_{E_k}\rangle$ are continuum states.

A bound state $|\psi_{E_n}\rangle$ can be normalized so that the norm becomes 1,

$$1 = \langle\psi_{E_n}|\psi_{E_n}\rangle = \int \mathrm{d}x\,|\chi_{E_n}(x)|^2 \tag{3.4}$$

where $|\chi(x)|^2$ may be interpreted as a probability density for the state. It is obviously time-independent.

3.2 Complex Energy and Momenta

If the energy E is allowed to be a complex number,

$$E = E_0 - i\frac{\Gamma}{2} \tag{3.5}$$

the norm (3.4) instead would become

$$\langle\psi_{E_0}|\psi_{E_0}\rangle = \int \mathrm{d}x\,(\psi_{E_0}(x,0))^2\,e^{-\frac{\Gamma}{\hbar}t}$$

[1] A stationary state is a state with a single definite energy, and which has a time-independent probability density.

which describes exponential decay. An attentive reader may have noted that the inner product used here was not the normal inner product, but rather a non-conjugated one. This is intentional, and the reason for this will become clear in the next section.

Using a complex energy is the basic idea behind describing tunneling in a time-independent framework. In this framework, a decaying state is neither bound nor unbound, and is called a *resonance*. In Section 3.4, we will see an example of a simple system that can harbor these resonant states.

Non-relativistically, the kinetic energy T and momentum k of a one-particle system are related by

$$T = \frac{\hbar^2 k^2}{2m}$$

where $\hbar$ is the Planck constant and m is the particle mass.

In order to convert from E to k, it is necessary to take the fractional power of an energy. By allowing E to be a complex number, k will be complex valued as well. The fractional power is a multivalued function on $\mathbb{C}$. To resolve this issue and make k single-valued, a branch-cut is introduced as in Figure 3.1. Using the branch cut in the figure (along the negative real axis) the energy sheet will be transformed into the right half-plane. This means that only k-values in the right half-plane are of physical interest. By using another Riemann surface, it is possible to also obtain k-values in the left half-plane. These are however not of any physical interest, and it is therefore assumed that the real part of k is nonnegative in the rest of this text. When later a choice of a momentum space basis is made, this assumption will implicitly be taken into account.

Since an energy may be negative and real, it is convenient to choose a branch cut slightly below the negative real axis. These values will then be transformed onto the positive imaginary axis by the square root function.

Consider now a particle of mass m and energy $E = \langle H \rangle = \langle T \rangle + \langle V \rangle$ in a system characterized by a potential $V(x)$, where $V(x) \to 0$ for $x \to \pm\infty$. There are three cases of interest here:

- The particle is not bound in the potential. This is a so-called continuum state. Since $\lim_{x\to\pm\infty} V(x) = 0$, $E_0 > 0$ in (3.5).
- The particle is bound inside the potential, a so-called bound state. $E_0 < 0$ and $\Gamma = 0$ in (3.5).
- The particle is neither bound nor unbound, and the probability of finding it inside the potential decays exponentially. This is a *resonant state*, with $E_0 > 0$ and $\Gamma > 0$.

These three different types of energies will be translated into the points in k-space indicated in Figure 3.2 by the $z^{\frac{1}{2}}$ map.

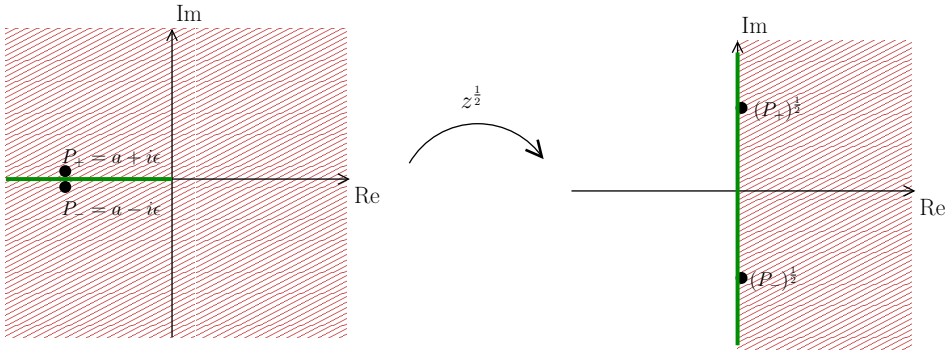

Figure 3.1. *Mapping of the complex plane, minus the negative real axis, onto itself, using one specific branch of the $z^{1/2}$ function. The other branch maps onto the left half plane.*

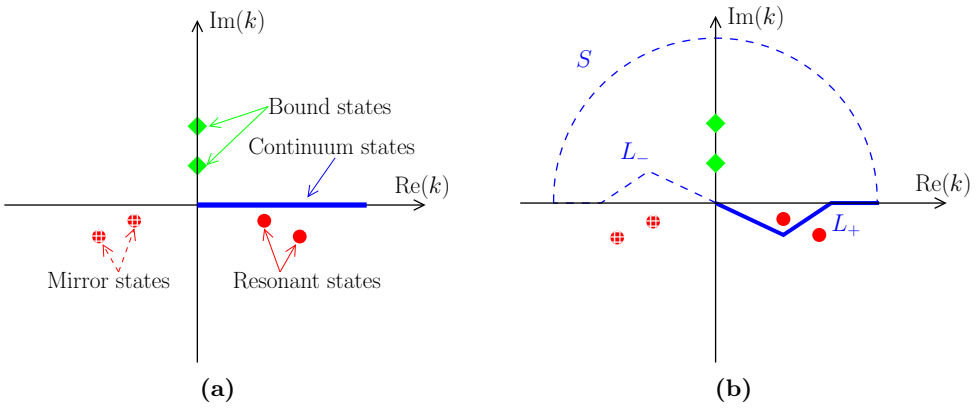

Figure 3.2. *Illustrations of different features in the complex momentum plane. (a) The location of poles corresponding to bound (green diamonds), resonance (red circles) and continuum (blue line) states in the k-plane. Also shown are the mirror states in the left half plane which are ignored. (b) The contour L_+ used in the Berggren completeness relation. The resonance state* above *the contour will be included in the sum for the completeness relation. Also shown are the contours L_- and S, which are used in conjunction with the Residue theorem to complete the proof of the Berggren completeness relation.*

A more thorough theoretical analysis would show that bound and resonant states would correspond to "poles" of the so-called S-matrix of the system. The S-matrix is a matrix relating initial and final states in a scattering process. For more details on this topic, see for example [9].

3.3 Berggren Completeness Relation

A key feature for this project is a complex-momentum single-particle basis known as the *Berggren basis*. In a paper from 1968 [10], the Swedish mathematician Tore Berggren showed that a complete basis can be constructed from the continuum states on the L_+ contour in Figure 3.2b, together with the resonant states above the contour and the bound states, using a *non-conjugated* inner product. This can be stated as the so-called *Berggren Completeness Relation*,

$$\sum_{\substack{\text{bound states}\\ \text{resonant states}}} |\psi_{E_n}\rangle \langle\psi_{E_n}| + \int_{L_+} \mathrm{d}k \, |\psi_{E_k}\rangle \langle\psi_{E_k}| = \mathbb{1}$$

The proof uses scattering theory, and is done in three dimensions. In the following, if nothing else is stated all momentum integrals are over the contour L_+.

3.3.1 Inner Product

In the rest of this work, all inner products are assumed to be without conjugation unless something else is stated. This means that the inner product of two states ψ_A and ψ_B can be expressed in the position basis as

$$\langle\psi_A|\psi_B\rangle = \int \mathrm{d}x \psi_A(x)\psi_B(x)$$

in contrast to the usual definition,

$$\langle\psi_A|\psi_B\rangle = \int \mathrm{d}x \psi_A^\dagger(x)\psi_B(x)$$

The underlying reason for this inner product is that a Hermitian operator only has real eigenvalues. In order to obtain complex energies, non-Hermitian quantum mechanics must therefore be used, which motivates changing the inner product.

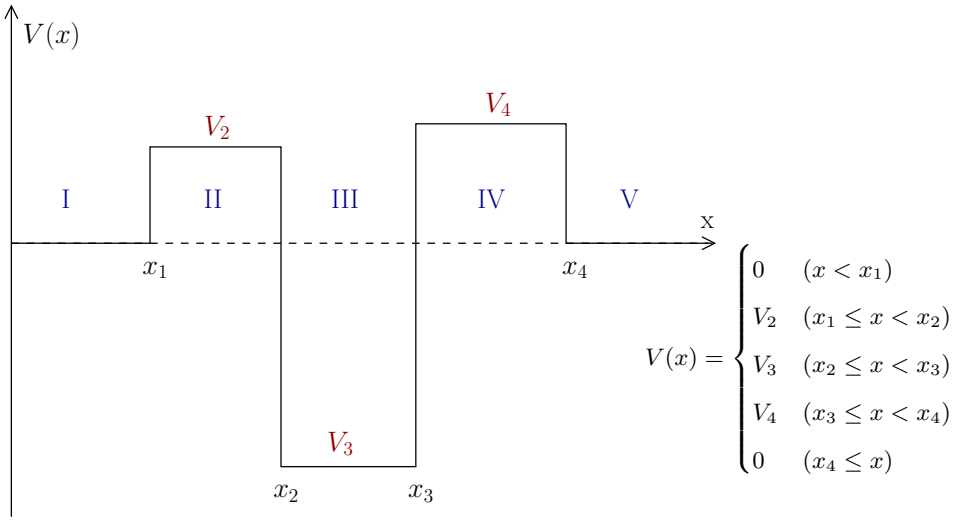

Figure 3.3. *An example of a piecewise constant potential, given by the expression $V(x)$.*

3.4 Piecewise Constant Potential

In this project, bound and resonant states will be found by introducing a basis expansion. However, for the case of a single particle in a piecewise constant potential, like the one depicted in Figure 3.3, a good approximation for the complex energy of both bound and resonant states can be obtained by a more intuitive method. This is also an important example, since its results can be used to verify the results obtained by means of the more involved basis expansion method.

A piecewise constant potential, such as the one in Figure 3.3, is a potential divided into N regions, where the potential is constant in each region. The leftmost and rightmost regions have the value zero and extends to positive and negative infinity, respectively. In the n:th region, corresponding to a potential V_n, we make the assumption that the particle is described by a plane wave with wavenumber given by $k_n = \frac{1}{\hbar}\sqrt{2m\,(E - V_n)}$. This is certainly true, and a standard textbook example, for purely real or imaginary k_n. Here however k_n is allowed to take almost any value in the right complex half-plane.

If the particle starts out as a bound or resonant state in some inner region of the potential, we make the ansatz wavefunction

$$\Psi_n(x) = \sum_{\sigma\in\{+,-\}} C_{n\sigma} e^{\sigma i k_n x}$$

where $C_{1+} = C_{N-} = 0$ since there is no incoming wave. At each intersection, the ansatz wavefunction is splined together to make the wavefunction and

its first derivative continuous. This amounts to $2N-2$ unknown variables, and the same number of linear equations for the unknown coefficients C. Therefore, a matrix equation $M\boldsymbol{c} = \mathbf{0}$ is obtained, and it will have nontrivial solutions for $\boldsymbol{c}$ exactly when the matrix M is singular. Since the coefficient matrix M is a function of the (possibly complex) energy $E = x + iy$ of the particle, one can define a function

$$\begin{aligned} &f(x,y) = |\mathrm{cond}\,(M(x+iy))| \\ &\mathbb{R}^2 \to \mathbb{R} \end{aligned}$$

where `cond` is the *condition number* of the matrix M. Obviously, $f(x,y) \geq 0$, and per definition the condition number is infinite when M is singular. The problem is thus reduced to finding the maxima of f, which can be located using some optimization method such as steepest ascent.

Comparison between the condition number of M and the results obtained by the basis expansion method can be found in Section 5.1.

3.5 Introducing a Basis Expansion

In order to transform the Schrödinger equation into an eigenvalue problem, a basis expansion method is employed. First, the completeness relation (3.3) is inserted into the time independent Schrödinger equation (3.2) for some eigenstate $|\Psi\rangle$ of the Hamiltonian H expressed in an *arbitrary basis* to obtain

$$\sum_{\text{bound states}} H\,|\psi_{E_n}\rangle\,\langle\psi_{E_n}|\Psi\rangle + \int_0^\infty \mathrm{d}k H\,|\psi_{E_k}\rangle\,\langle\psi_{E_k}|\Psi\rangle = E\,|\Psi\rangle \tag{3.6}$$

Projecting onto another energy eigenstate $\left|\psi_{E_{k'}}\right\rangle$, which we for simplicity assume to be a continuum state, gives

$$\int_0^\infty \mathrm{d}k \left\langle\psi_{E_{k'}}\middle|H\middle|\psi_{E_k}\right\rangle \langle\psi_{E_k}|\Psi\rangle = E\left\langle\psi_{E_{k'}}\middle|\Psi\right\rangle \tag{3.7}$$

Discretizing (3.7) will lead to a matrix equation, as we shall see.

3.6 Momentum Space Basis

In order to proceed from Equation (3.7) in momentum space, a suitable choice of momentum space basis is made. The momentum space basis should consist of eigenstates for the kinetic operator. Furthermore, any (orthonormal) basis $\{a\}$ must fullfill the condition

$$\left\langle a\middle|a'\right\rangle = \delta\left(a - a'\right)$$

using the appropriate inner product. Due to the non-conjugated inner product, it is necessary to make sure that this condition is fulfilled.

The chosen basis is

$$\left\langle x \middle| \mathfrak{B}_k^i \right\rangle = \begin{cases} \sqrt{\frac{2}{\pi}} \sin(kx) & (i=0) \\ \sqrt{\frac{2}{\pi}} \cos(kx) & (i=1) \end{cases} \tag{3.8}$$

bearing in mind that $\mathfrak{Re}\,(k) \geq 0$. In order to show the orthogonality properties, the inner product between the elements is computed. Expressing this in the position basis, so that

$$\left\langle \mathfrak{B}_{k_1}^{i_1} \middle| \mathfrak{B}_{k_2}^{i_2} \right\rangle = \int \mathrm{d}x \left\langle \mathfrak{B}_{k_1}^{i_1} \middle| x \right\rangle \left\langle x \middle| \mathfrak{B}_{k_2}^{i_2} \right\rangle$$

directly gives

$$\frac{2}{\pi} \int_{-\infty}^{\infty} \mathrm{d}x \sin(k_i x) \sin(k_j x) = \delta\left(k_i - k_j\right) + \delta\left(k_i + k_j\right) = \delta\left(k_i - k_j\right) \tag{3.9a}$$

$$\frac{2}{\pi} \int_{-\infty}^{\infty} \mathrm{d}x \cos(k_i x) \cos(k_j x) = \delta\left(k_i - k_j\right) + \delta\left(k_i + k_j\right) = \delta\left(k_i - k_j\right) \tag{3.9b}$$

$$\frac{2}{\pi} \int_{-\infty}^{\infty} \mathrm{d}x \cos(k_i x) \sin(k_j x) = 0 \tag{3.9c}$$

where the last equality on each line comes from $\mathfrak{Re}\,(k) \geq 0$, observing that no k-values will be on the negative imaginary axis due to the choice of branch cut and also noting that the momentum is never zero, so $k \neq 0$.

Here it is also appropriate to note the resemblance between the choice of basis and a common choice of plane wave basis, e^{ikx}. We are trying to describe a one-dimensional decaying state, and intuitive choice would therefore be a basis that consists of a sum of plane waves travelling to the left and plane waves travelling to the right. Indeed, the trigonometric functions cos and sin can be expressed as

$$\cos(kx) = \frac{e^{ikx} + e^{-ikx}}{2}$$

$$\sin(kx) = \frac{e^{ikx} - e^{-ikx}}{2i}$$

An important difference between the one-dimensional and three-dimensional description of a quantum mechanical system, is that in three dimensions, the radial coordinate is always positive. Here, x may take on any real value.

The choice of basis made here is not the only possible choice. Since the relevant potential (2.3) tends to ∞ fast when $x \to -\infty$, the wavefunction

should tend to zero fast for decreasing x. This could be exploited by solving the Schrödinger equation with an infinite "wall" to the left, which imposes a condition that the wavefunction becomes zero there. Essentially, one could then remove half the number of basis vectors. This has in fact been attempted, but it turned out to require about twice the number of basis states compared to the basis (3.8) in order to numerically stabilize the positions of the resonances in the complex plane[2]. Therefore, the practical gain was negligible.

For brevity we introduce the notation $\sin \equiv \mathrm{trig}^0$ and $\cos \equiv \mathrm{trig}^1$ which will be used in the following sections.

3.7 One Particle Basis Expansion

In order to solve the Schrödinger equation for a single particle, we start from the Hamiltonian for a particle in a one-dimensional potential,

$$H = \frac{p^2}{2m} + V$$

where p is the momentum operator, m is the mass and V is the potential operator. This is inserted into Equation (3.6), using the basis (3.8), to obtain

$$\left\langle \mathfrak{B}_{k_1}^{i_1} \middle| V \middle| \mathfrak{B}_{k_2}^{i_2} \right\rangle = \int \mathrm{d}x_1 \mathrm{d}x_2 \left\langle \mathfrak{B}_{k_1}^{i_1} \middle| x_1 \right\rangle \langle x_1 | V | x_2 \rangle \left\langle x_2 \middle| \mathfrak{B}_{k_2}^{i_2} \right\rangle =$$
$$= \int \mathrm{d}x V(x) \mathrm{trig}^{i_1}(k_1 x) \mathrm{trig}^{i_2}(k_2 x) \equiv V(k_1, i_1, k_2, i_2)$$

and

$$\left\langle \mathfrak{B}_{k_1}^{i_1} \middle| \frac{p^2}{2m} \middle| \mathfrak{B}_{k_2}^{i_2} \right\rangle = \frac{\hbar^2}{2m} \frac{2}{\pi} \int \mathrm{d}x_1 \mathrm{d}x_2 \mathrm{trig}^{i_1}(k_1 x_1) \, \delta(x_1 - x_2) \, \frac{\partial^2}{\partial x_2^2} \mathrm{trig}^{i_2}(k_2 x_2) =$$
$$= -\frac{\hbar^2 k_2^2}{2m} \frac{2}{\pi} \int \mathrm{d}x_1 \mathrm{d}x_2 \delta(x_1 - x_2) \, \mathrm{trig}^{i_1}(k_1 x_1) \, \mathrm{trig}^{i_2}(k_2 x_2) =$$
$$= -\frac{\hbar^2 k_2^2}{2m} \int \mathrm{d}x_1 \mathrm{d}x_2 \delta(x_1 - x_2) \left\langle \mathfrak{B}_{k_1}^{i_1} \middle| x_1 \right\rangle \left\langle x_2 \middle| \mathfrak{B}_{k_2}^{i_2} \right\rangle =$$
$$= -\frac{\hbar^2 k_2^2}{2m} \int \mathrm{d}x_1 \left\langle \mathfrak{B}_{k_1}^{i_1} \middle| x_1 \right\rangle \left\langle x_1 \middle| \mathfrak{B}_{k_2}^{i_2} \right\rangle = -\frac{\hbar^2 k_2^2}{2m} \left\langle \mathfrak{B}_{k_1}^{i_1} \middle| \mathfrak{B}_{k_2}^{i_2} \right\rangle =$$
$$= -\frac{\hbar^2 k_2^2}{2m} \delta(k_1 - k_2) \, \delta_{i_1, i_2}$$

where the position space representation of the momentum operator was used.

Inserting this into Equation (3.6) gives

[2]Since the resonances are physical, their position should be independent on the choice of contour L_+, if the number of basis states is large enough and the choice of contour is "reasonable". This is further discussed in Chapter 4.

$$\sum_{i_2\in\{1,2\}}\int \mathrm{d}k_2 \left[-\frac{\hbar^2 k_2^2}{2m}\delta\left(k_1-k_2\right)+V(k_1,i_1,k_2,i_2)\right]\left\langle \mathfrak{B}_{k_2}^{i_2}\middle|\Psi\right\rangle =$$
$$=E\left\langle \mathfrak{B}_{k_1}^{i_1}\middle|\Psi\right\rangle$$

or

$$-\frac{\hbar^2 k_1^2}{2m}\left\langle \mathfrak{B}_{k_1}^{i_1}\middle|\Psi\right\rangle+\sum_{i_2\in\{1,2\}}\int \mathrm{d}k_2 V(k_1,i_1,k_2,i_2)\left\langle \mathfrak{B}_{k_2}^{i_2}\middle|\Psi\right\rangle =$$
$$=E\left\langle \mathfrak{B}_{k_1}^{i_1}\middle|\Psi\right\rangle$$

A so-called quadrature rule is now used to discretize the integral over k_2. A quadrature rule is essentially a rule that approximates a definite integral by a weighted sum, so that

$$\int_a^b \mathrm{d}x f(x)\approx\sum_{i=0}^{N-1} w_i f(x_i)$$

where the w_i:s are the weights for the sum. A more thorough explanation of quadrature rules is given in Appendix A. Applying the rule gives

$$-\frac{\hbar^2 (k_1^m)^2}{2m}\left\langle \mathfrak{B}_{k_1^m}^{i_1}\middle|\Psi\right\rangle+\sum_{i_2\in\{1,2\}}\sum_{n=0}^{N/2-1} w_n V(k_1^m,i_1,k_2^n,i_2)\left\langle \mathfrak{B}_{k_2^n}^{i_2}\middle|\Psi\right\rangle =$$
$$=E\left\langle \mathfrak{B}_{k_1^m}^{i_1}\middle|\Psi\right\rangle . \tag{3.10}$$

In order to further simplify, some new notation is handy. The k:s and i:s are grouped together to pairs, (k_a,i_a), $a\in\{1,2\}$. An *ordering* of the pairs is then introduced, such that the pairs with lower i preceeds the pair with higher i. A k corresponding to a smaller value of the parameter on the contour along which we are integrating preceeds a k corresponding to a larger parameter value if the i:s are equal. Since there are $N/2$ k:s and 2 i:s, there will be N such pairs. By replacing the k:s and the i:s with an index simply referring to the pair, we simplify the notation. If (k_1,i_1) corresponds to the i:th pair and (k_2,j_2) to the j:th pair, we denote $\left\langle \mathfrak{B}_{k_1^m}^{i_1}\middle|\Psi\right\rangle\equiv\phi_i$ and $V(k_1^m,i_1,k_2^n,i_2)\equiv V_{ij}$. The above expression (3.10) then simplifies to

$$-\frac{\hbar^2 (k_1^m)^2}{2m}\phi_i+\sum_{j=0}^{N-1} w_j V_{i,j}\phi_j = E\phi_i$$

or

$$\sum_{j=0}^{N-1}\left[-\frac{\hbar^2 k_i^2}{2m}\delta_{ij}+w_j V_{ij}\right]\phi_j = E\phi_i \tag{3.11}$$

Defining H_{ij} as

$$H_{ij} = -\frac{\hbar^2 k_i^2}{2m}\delta_{ij}+w_j V_{ij}$$

transforms Equation (3.11) into

$$\sum_{j=0}^{N-1} H_{ij}\phi_j = E\phi_i \tag{3.12}$$

which can be recognized as an eigenvalue problem.

The matrix H is nonsymmetric due to the term w_j in front of V. It can be symmetrized by redefining $\tilde{\phi}(k_i) = \sqrt{w_i}\phi(k_i)$ and $\tilde{H}_{ij} = \sqrt{\frac{w_i}{w_j}}H_{ij}$ which will give us the equation

$$\sum_{j=0}^{N-1}\tilde{H}_{ij}\tilde{\phi}(k_j) = E\tilde{\phi}(k_i)$$

with

$$\tilde{H}_{ij} = \frac{\hbar^2 k_i^2}{2m}\delta_{ij}+\sqrt{w_i w_j}V_{ij} \tag{3.13}$$

which is symmetric under the change $i \leftrightarrow j$. Note however that $\tilde{H}$ is not in general Hermitian, since V_{ij} is a complex number.

3.8 Harmonic Oscillator Basis

A common basis in quantum mechanics is the harmonic oscillator basis. In this thesis it is used both for purposes of introducing a suitable cutoff for the interaction, but also for purposes of verifying the correctness of the program code used in calculations. The harmonic oscillator basis states are the eigenfunctions $|n\rangle$ of the Hamiltonian

$$H = -\frac{\hbar^2}{2m}\frac{\partial^2}{\partial x^2}+\frac{1}{2}m\omega^2 x^2$$

which in position space are given by

$$\langle x|n\rangle \equiv \phi_n(x) = \frac{1}{\sqrt{2^n n!}}\left(\frac{m\omega}{\pi\hbar}\right)^{1/4}\cdot e^{-\frac{m\omega x^2}{2\hbar}}\cdot H_n\left(\sqrt{\frac{m\omega}{\hbar}}x\right)$$

where H_n is the n:th Hermite polynomial, defined by

$$H_n(x) = (-1)^n e^{x^2}\frac{\mathrm{d}^n}{\mathrm{d}x^n}e^{-x^2} \tag{3.14}$$

3.9 Many-Body Basis Expansion

The Hilbert space for many particles can be generated as a tensor product of the single-particle Hilbert spaces. For N particles with associated single-particle Hilbert spaces $\mathcal{H}_1, \ldots, \mathcal{H}_N$, the total Hilbert space is given by

$$\mathcal{H}_{\text{tot}} = \mathcal{H}_1 \otimes \mathcal{H}_2 \otimes \cdots \otimes \mathcal{H}_N$$

The many-body state is then given by a tensor product of the single-particle states, that is,

$$|\Psi_{\text{tot}}\rangle = |\psi_1\rangle \otimes |\psi_2\rangle \otimes \cdots \otimes |\psi_N\rangle \equiv |\psi_1 \psi_2 \ldots \psi_N\rangle$$

In our case, all particles are distinguishable, which means that there is no need for antisymmetrization.

One could now proceed to construct the many-body basis from the individual single-particle momentum basis states described above. This approach may however not be the best, in the sense that an unmanageable number of basis elements must be included in order to get a good description of the many-body state.

Instead, as a basis for the single-particle Hilbert spaces a basis constituting of the solutions to the single-particle problems is chosen. It can be shown [10] that this is indeed a complete basis. For a particle p, these basis states will be labeled as $\left\{\psi_p^n\right\}_{n=0}^{N-1}$ for the rest of this section.

In the context of this thesis, at most 2 particles are treated. The coupling between particles is treated as a delta function interaction. The interaction only affects the particles if they are in different states. The treatment is thus restricted to the case of one particle in state $|\uparrow\rangle$ and one in state $|\downarrow\rangle$. The common state of these is denoted $|\uparrow\downarrow\rangle = |\uparrow\rangle \otimes |\downarrow\rangle$.

The Hamiltonian for the system can be written as the sum of the individual one-particle Hamiltonians, plus an interaction term as described in Section 3.10:

$$H_{\uparrow\downarrow} = H_\uparrow + H_\downarrow + V_{\uparrow\downarrow} \tag{3.15}$$

Evaluating this in a two-particle basis gives

$$\begin{aligned} \left\langle \psi_1^a \psi_2^b \middle| H_{12} \middle| \psi_1^c \psi_2^d \right\rangle &= \langle \psi_1^a | H_1 | \psi_1^c \rangle \, \delta_{bd} + \left\langle \psi_1^b \middle| H_2 \middle| \psi_1^d \right\rangle \delta_{ac} \\ \left\langle \psi_1^a \psi_2^b \middle| V_{\uparrow\downarrow} \middle| \psi_1^c \psi_2^d \right\rangle &= \delta_{ac}\delta_{bd} \left(E_a + E_b\right) + V_{abcd} \equiv H_{abcd} \end{aligned} \tag{3.16}$$

It will turn out that V_{abcd} is symmetric under $a \leftrightarrow c$ and $b \leftrightarrow d$, and therefore H_{abcd} will also be symmetric under these changes. This does in fact save much computational work.

3.10 Two-Particle Contact Interaction

In order to model several particles, an interaction term will need to be added to the Hamiltonian. This interaction term, written $V_{\uparrow\downarrow}$, is modelled as a contact interaction, which is defined in position space as

$$\langle x_1' x_2' | V_{\uparrow\downarrow} | x_1 x_2 \rangle = g\delta(x_1 - x_2)\,\delta(x_1' - x_1)\,\delta(x_2' - x_2) \tag{3.17}$$

where g is the *coupling coefficient*, determining the interaction strength.

If a basis $\{\psi_p^n\}_{n=0}^{N-1}$, where p denotes the particle species ($p \in \{1,\ 2\}$) is expressible in coordinate space as $\psi_p^n(x) \equiv \langle x | \psi_p^n \rangle$, this matrix element can be written as

$$\begin{aligned} V_{abcd} \equiv& \left\langle \psi_1^a \psi_2^b \middle| V_{\uparrow\downarrow} \middle| \psi_1^c \psi_2^d \right\rangle = \\ =& g \int_{-\infty}^{\infty} \mathrm{d}x \psi_1^a(x) \psi_2^b(x) \psi_1^c(x) \psi_2^d(x) \end{aligned} \tag{3.18}$$

Using a position space basis, this is however not guaranteed to converge, due to the asymptotic behavior of the basis states. If the energy is complex, these will blow up at infinity.

One could decide to substitute $\pm\infty$ in the integral for some cutoff value x_{cut} in order to obtain some number. Instead, another method is used to make sure a finite value is obtained: the basis states and the matrix elements are projected onto harmonic oscillator states. That is, complete sets of two-body harmonic oscillator states are inserted in the expression for the interaction:

$$\begin{aligned} &\left\langle \psi_1^a \psi_2^b \middle| V_{\uparrow\downarrow} \middle| \psi_1^c \psi_2^d \right\rangle = \\ &= \sum_{\substack{n_1,n_2 \\ n_3,n_4}} \left\langle \psi_1^a \psi_2^b \middle| n_1 n_2 \right\rangle \langle n_1 n_2 | V_{\uparrow\downarrow} | n_3 n_4 \rangle \left\langle n_3 n_4 \middle| \psi_1^c \psi_2^d \right\rangle \end{aligned} \tag{3.19}$$

Thereafter, some cutoff $n_{\max}$ is imposed on the values of n_1, n_2, n_3 and n_4, so that $0 \leq n_1, n_2, n_3, n_4 \leq n_{\max}$ in the sum. This is a so-called *regularization method* for the integral. It should be noted that if the basis states $\{\psi_p^n\}_{n=0}^{N-1}$ are chosen as harmonic oscillator basis states, one would obtain the correct bound states with this approach.

It should be noted that the summand in the expression above can be factored as

$$\left\langle \psi_1^a \middle| n_1 \right\rangle \left\langle \psi_2^b \middle| n_2 \right\rangle \left\langle \psi_1^c \middle| n_3 \right\rangle \left\langle \psi_2^d \middle| n_4 \right\rangle \langle n_1 n_2 | V_{\uparrow\downarrow} | n_3 n_4 \rangle \tag{3.20}$$

where a term

$$\left\langle \psi_j^k \middle| n_p \right\rangle = \int_{-\infty}^{\infty} \mathrm{d}x \psi_j^k(x) \phi_n(x) \tag{3.21}$$

and the interaction element in harmonic oscillator coordinates can be written

$$\langle n_1 n_2 | V_{\uparrow\downarrow} | n_3 n_4 \rangle = g \int_{-\infty}^{\infty} \mathrm{d}x \phi_{n_1}(x) \phi_{n_2}(x) \phi_{n_3}(x) \phi_{n_4}(x) \tag{3.22}$$

This factorization makes it possible to create lookup tables of elements, and then compute the sum with only values from these tables. This vastly improves the performance of computations, and brings the timescale down to reasonable times.

Also notable is that V_{abcd} is symmetric under the index changes $a \leftrightarrow c$ and $b \leftrightarrow d$, which can be seen from the definition above.

3.11 Enumerating Many-Particle States

In order to write (3.16) as an eigenvalue equation, the basis (and thereby also H_{abcd}) needs to be "flattened out". This is done by introducing an ordering of the eigenvectors. Each pair of basis states can be described by two indices (a, b), $a, b \in \{0, \cdots, N-1\}$. These N^2 pairs can be ordered in any arbitrary well-defined way. For instance, we may choose to first order by the first index, and then order by the second index, preserving the first-index ordering. This can be done by taking $i \in \left\{0, \cdots, N^2 - 1\right\}$, and

$$\begin{aligned} a &\equiv i \bmod N \\ b &\equiv \left\lfloor \frac{i}{N} \right\rfloor \end{aligned}$$

This is convenient, since it makes it possible to describe any two-particle state by a single index i. Denote such a state by ϕ_i. The enumeration also allows describing any element of the Hamiltonian with two indices, which can be denoted by i and j. The Hamiltonian thus has two-indices, and can be represented by a matrix H_{ij}. This matrix is symmetric, since $i \leftrightarrow j$ corresponds to $a \leftrightarrow c$ and $b \leftrightarrow d$. The eigenvalue equation to solve is then

$$\sum_{j=0}^{N^2-1} H_{ij} \phi_j = E \phi_i \tag{3.23}$$

which should be contrasted to Equation (3.12).

3.12 Harmonic Oscillator Potential

For two particles in a one-dimensional harmonic oscillator potential, interacting with a delta function interaction, there is an analytical expression for the energy spectrum of the particles. In absolute numbers, expressed in

multiples $\hbar\omega$ of harmonic oscillator units, and with the interaction as above with g in units of $\sqrt{\frac{\hbar}{\omega m}}$, this expression reads

$$E_{\text{total}} = E_{\text{int}} + n + \frac{1}{2} \tag{3.24}$$

where the relative energy E_{int} is given by [11]

$$\frac{\Gamma\left(-E_{\text{int}}/2 + 1/4\right)}{\Gamma\left(-E_{\text{int}}/2 + 3/4\right)} = -\frac{2}{g} \tag{3.25}$$

for an interacting state, and $E_{\text{int}} = \frac{3}{2}$ for a noninteracting state. n is any integer, representing the center of mass excitations.

This relation is important for the purpose of verifying the correctness of the computational routines for two interacting particles, as will be further described in Section 5.3. The energy levels, both calculated from this equation and by using the basis expansion method, can be found in Figure 5.4.

3.13 Perturbative Solutions

For a weak inter-particle interaction, the off-diagonal matrix elements of the matrix corresponding to (3.15) may be small compared to the diagonal elements. The energy and decay rate of a state consisting of two interacting particles may then be approximated by means of perturbation theory. Let i denote the diagonal the index of the two-particle state with both particles in the resonant state, as described by Section 3.11. Viewing the off-diagonal matrix elements in (3.23) as a perturbation, the energy E_i can then be approximated to third order by [12]

$$E_i \approx \underbrace{H_{ii}}_{\text{0th order}} + \underbrace{\sum_{j \neq i} \frac{H_{ij}^2}{H_{ii} - H_{jj}}}_{\text{2nd order}} . + \underbrace{\sum_{\substack{j \neq i \\ k \neq i,j}} \frac{H_{ij} H_{jk} H_{ki}}{\left(H_{ii} - H_{jj}\right)\left(H_{ii} - H_{kk}\right)}}_{\text{3rd order}} . \tag{3.26}$$

Chapter 4

Implementation

In this chapter, details on how the theory is used for practical calculations is discussed. First, the procedure for obtaining single- and two-particle energies and tunneling rates is described. Thereafter, the potential cutoff is introduced. This is a crucial modification made to the potential (2.3) in order for the basis expansion method to produce valid results. The chapter is concluded by mentioning some other practical considerations taken into account when realizing the procedures into software for actually performing computations.

4.1 Single-Particle Solutions

To obtain the single-particle solution, there are four primary steps that should be taken:

1. Construct a discretized momentum basis along the contour L_+.
2. Construct the matrix representation of the Hamiltonian for the system described in this basis.
3. Solve for the eigenvalues, and optionally eigenvectors, of the matrix.
4. Identify the resonance state(s) from the eigenvalues.

The first step is done using a Gauss-Legendre quadrature rule on each of the segments of L_+, and with a basis as described in Section 3.6. The number of points on each segment, as well as the start- and endpoints of the segments therefore needs to be determined. The shape of L_+ (segment start- and endpoints) can be roughly estimated using the expected energy range for each particle, which can be done by hand using a harmonic oscillator approximation. The number of points has to be determined using trial and error, if enough points are chosen the value of any resonance should be stable with respect to reasonable changes of the contour shape.

In the second step, Equation (3.13) is used for the construction of the Hamiltonian.

The third step is typically performed by using an eigenvalue solver, such as `LAPACK` (see Appendix B). Since the number of rows and columns in the matrix is typically in the order of a few hundred, this tends to be fast.

The fourth step is carried out visually. The eigenvalues are first converted to the corresponding momentum values. The resonance states can then easily be identified by inspection, since their position in the k-plane are in the 4:th quadrant and a bit off from the contour. Also, a simple heuristic algorithm was developed to allow for automatic detection of resonances from the spectra.

Since a resonant state is physical, it should also be independent of the shape of the contour, which can be used to verify that a point in the complex plane indeed corresponds to a resonance. This clearly distinguishes the state from other solutions, which will follow the contour closely. These so-called *scattering states* correspond to free-particle solutions (particles never bound by the trap) of the Schrödinger equation.

4.2 Two Particle Solutions

For two (or more) particles, one first finds the one-particle solutions mentioned above for each particle, including finding the eigenvectors. In this thesis, many particles means that two particles are considered.

After finding the single-particle eigenvalues and eigenvectors, the following four steps are performed:

1. Calculate the interaction for the basis states in the many-particle basis.
2. Construct the matrix for the many-particle Hamiltonian expressed in this basis.
3. Solve for the eigenvalues, and optionally eigenvectors, of the matrix.
4. Identify the resonance state.

In the first step, the interaction element is computed from Equation (3.19), using equations (3.20) to (3.22). After that, the many-particle Hamiltonian is constructed from Equation 3.16.

The matrix size is the square of the matrix size used for the single-particle cases. This poses a problem, since this means a very large matrix. Therefore, one may need to resort to iterative algorithms for finding single eigenvalues. This is further described in Appendix B.

The resonance states may be identified in the k-plane, in a similar fashion as the one-particle case. However, it is not so obvious which k-value corresponds to a two-particle resonance, an issue illustrated by Figure 4.1. This

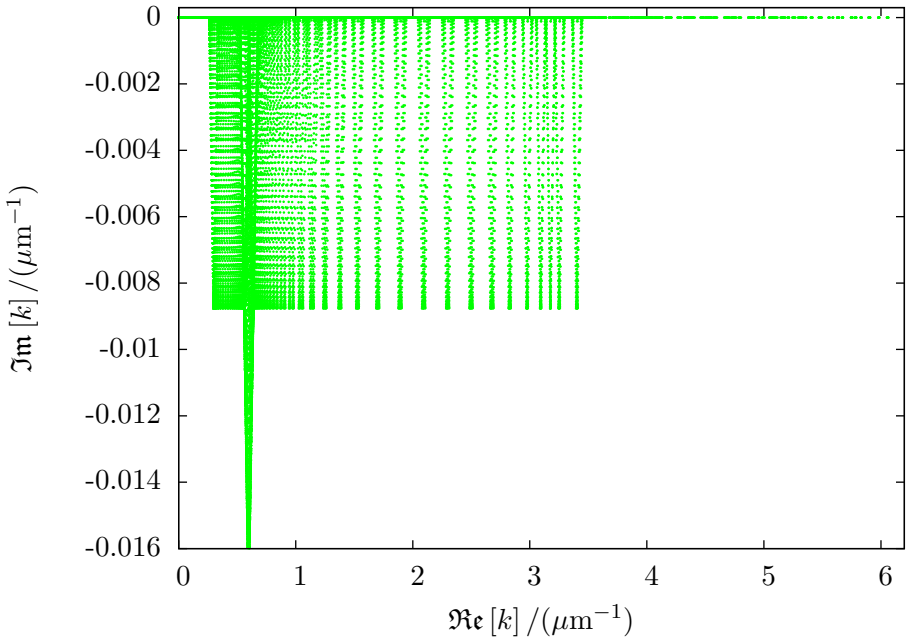

Figure 4.1. *Location of solutions to the two-particle Schrödinger equation in the complex k-plane.*

figure shows the solutions to the Schrödinger equation for two interacting particles.

A method that can be used to identify the resonance is to overlay the spectra from the solution with multiple different contours. Since the resonance is physical, it should be independent on the choice of contour.

Another approach is to use the zero-interaction two-particle wavefunction corresponding to both particles in the resonant state as a starting vector in an interative eigenvalue algorithm. For a small coupling coefficient, the algorithm may then converge towards the eigenvalue of the interacting system. The convergence is under the condition of using a moderate number of iterations and restarting the algorithm with the vector giving most overlap with the previous one, after finding only a few eigenvectors. The value found by this method can then be used as input for a more exact shift-inverted Arnoldi algorithm (see Appendix B).

A found eigenstate may also be checked by observing its overlap with the zero-interaction wavefunction. For a weak coupling, the resonance wavefunction should be dominated by the component with both particles in the single-particle resonant state.

In practice, all these methods are used in conjunction to achieve greater certainty considering which of the solutions to the eigenvalue problem corresponds to the physical resonance.

4.3 Potential Cutoff

The value of the potential described in (2.3) tends to $\pm\infty$ when $z \to \pm\infty$. This poses a problem in the numerical calculations since this would make all integrals undefined. The solution to this problem is to introduce a cutoff at both the left and the right side. In practice, this means that we define a new potential $\tilde{V}(z)$ by

$$\tilde{V}(z) \equiv \begin{cases} V(z) + R_0 & (a \leq z \leq b) \\ 0 & (\text{otherwise}) \end{cases} \tag{4.1}$$

where R_0 is a constant energy shift, b is chosen in such a way that when the value of the potential becomes zero, it stays zero thereafter. R_0 is chosen such that this point is relatively far to the right, typically $15 - 20\,\mu$m. a is chosen to an arbitrary negative value, typically about $-2\,\mu$m. In order to make sure that the values of a, b and R_0 did not influence the final result, different choices of these were tried, and if a is far enough to the left and b far enough to the right, the result seems to be largely independent on this choice, see Section 6.3.

4.4 Practical Considerations

There are several practical considerations taken into account when writing software to implement the methods described in Section 4.1 and 4.2, some of which are mentioned here.

4.4.1 Software Verification

The software for the numerical calculations was written in a modular fashion in order to make unit testing of its individual components possible. These tests were typically implemented at an early stage and executed automatically each time the program compiled, to verify the consistency of any changes with the expected behavior.

Furthermore, verification was carried out by comparing results obtained by the basis expansion method with results obtained by other means, and by other authors. These comparisons are further described in Chapter 5. The comparative verification is important, since it strongly suggests that the Berggren basis does indeed work in one dimension and that the results are reliable.

4.5 Finding Eigenvalues

Much literature is availiable on how to numerically find eigenvalues and eigenvectors. In this project, two different approaches were used: shifted

QR iteration (provided by `LAPACK`) and restarted Krylov subspace methods (mainly Arnoldi iteration provided by `ARPACK`). More details on these algorithms, as well as further references on them, can be found in Appendix B.

4.5.1 Memory

When solving for energies and eigenvalues for more than one particle, memory becomes an issue. Since the many-particle basis contains all possible combinations of the single-particle basis states, the number of elements in the two-particle matrix will be equal to the number of elements in the single-particle matrix to the power of two. For a modest number of 200 single-particle basis states, this equals to $1.6 \cdot 10^9$ matrix elements. Representing each element as a complex number with double precision equals to 16 bytes per element, which yields almost 24 Gb (plus any overhead) when representing the matrix in the computer's memory. Furthermore, in order to compute eigenvalues and eigenvectors of the matrix, even more space is required, typically two to three times this space extra is required during the computation process in order to store intermediate factorizations and output values. This ultimately puts an upper limit on the amount of basis states that can be used, imposed by the available hardware. These limitations will be further discussed in Chapter 7.

Chapter 5

Benchmarking

In this section, some benchmarks are presented. The main purpose of these is to verify the correctness of the program code used in the computations.

5.1 Piecewise Constant Potential

The method described in Section 3.4 was applied to different piecewise constant potentials, and the result was compared to the result obtained by a basis expansion method. An example of this comparison is shown in Figure 5.1, where the potential in Figure 5.2a was used. As can be seen from the figure, the result obtained by maximizing a matrix condition number is in strong agreement with the result obtained by means of our basis expansion method. Applying a steepest-ascent approach in the neighborhood of the poles in this case gives results differing less than 0.1% for the bound states and less than 1% for both the real and imaginary part of the resonant state.

Figure 5.2b shows the wavefunctions corresponding to the two bound and deepest resonance state in the potential in Figure 5.2a. The bound-state solutions, corresponding to purely imaginary k, have an increasing number of nodes. The resonance at a first glance looks like a bound state with an additional node, but its wavefunction does *not* go to zero outside the potential ($|z| > 1$).

5.2 Single Particle in a Similar Potential

An important verification of the software used for the computations is comparision with other known results. In a paper by Hazi and Taylor [13], the

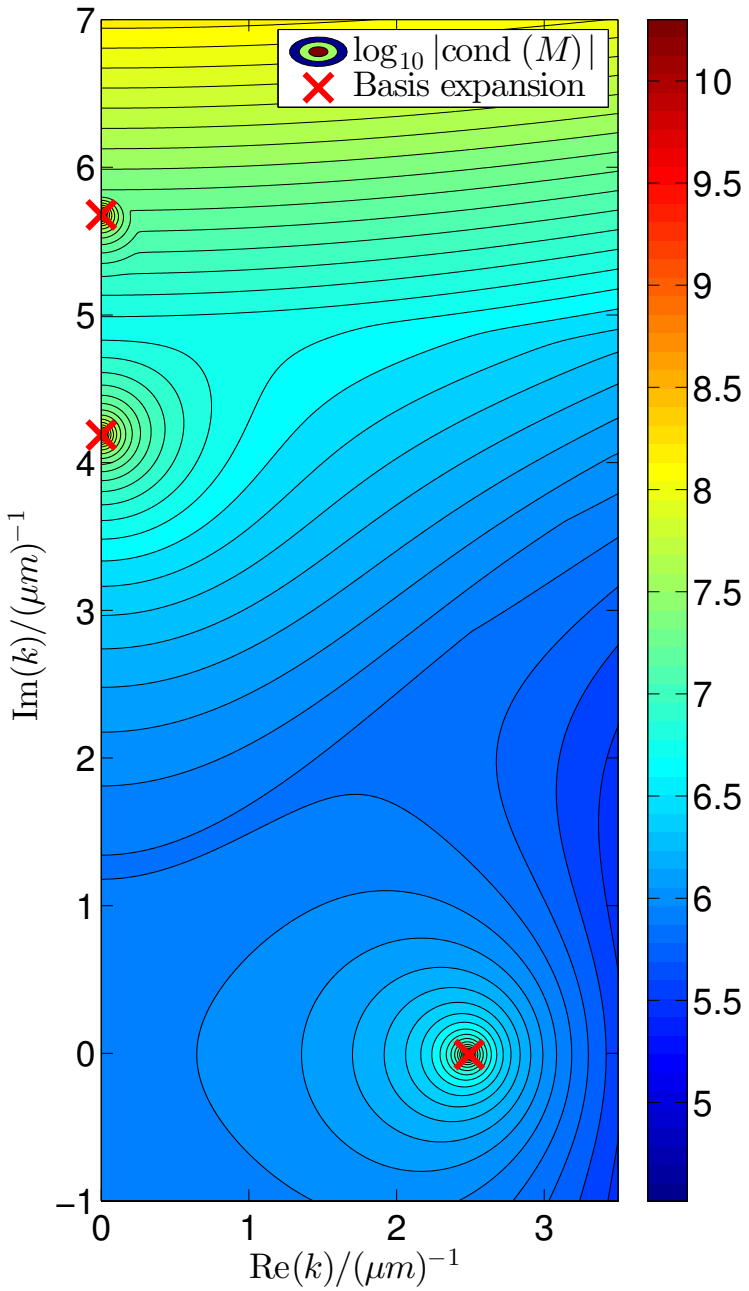

Figure 5.1. *Location of poles for a potential like in Figure 3.3, with* $(x_1, x_2, x_3, x_4) = (-1.0, -0.6, 0.6, 1.0)\,\mu\mathrm{m}$ *and* $(V_1, V_2, V_3) = (2.2, -1.5, 2.2)\,\mu\mathrm{K}\cdot\mathrm{k_B}$. *The potential and pole wavefunctions are shown in Figure 5.2.*

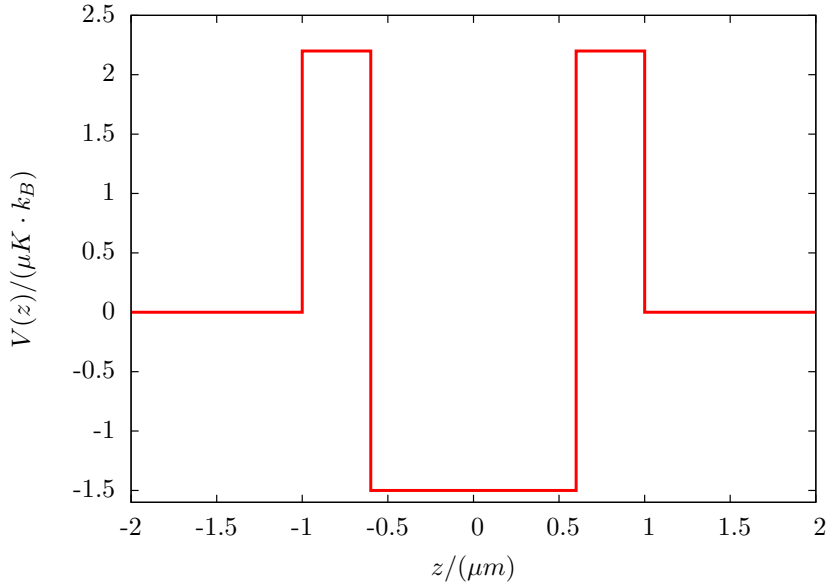

(a)

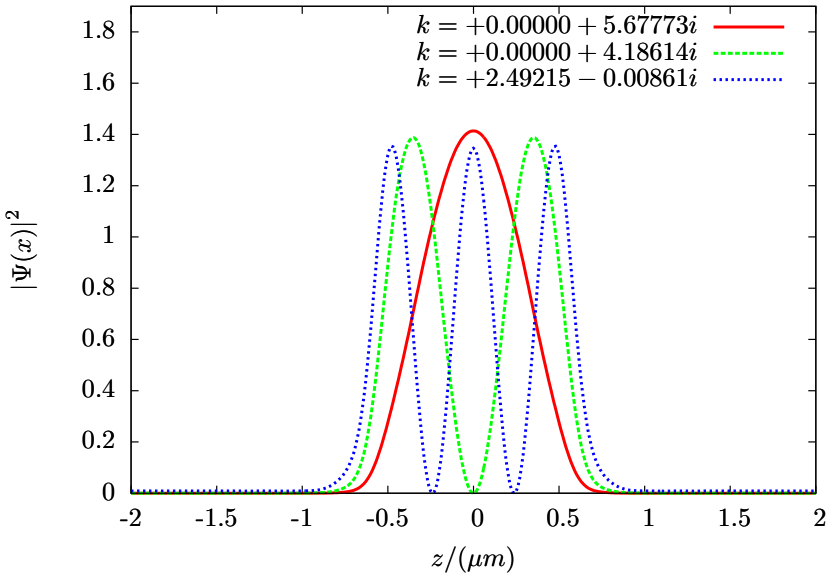

(b)

Figure 5.2. *(a) Potential to which the poles in Figure 5.1 correspond. (b) Modulus square of the wavefunctions for the poles in Figure 5.1.*

energies and line widths for resonances in the potential

$$V(x) = \begin{cases} \frac{1}{2}x^2 & (x < 0) \\ \frac{1}{2}x^2 e^{-\lambda x^2} & (x \geq 0) \end{cases} \tag{5.1}$$

where $\lambda > 0$ (see Figure 5.3) are computed and discussed in detail. This potential shares some main features with the trap potential (2.3) of the Heidelberg experiment.

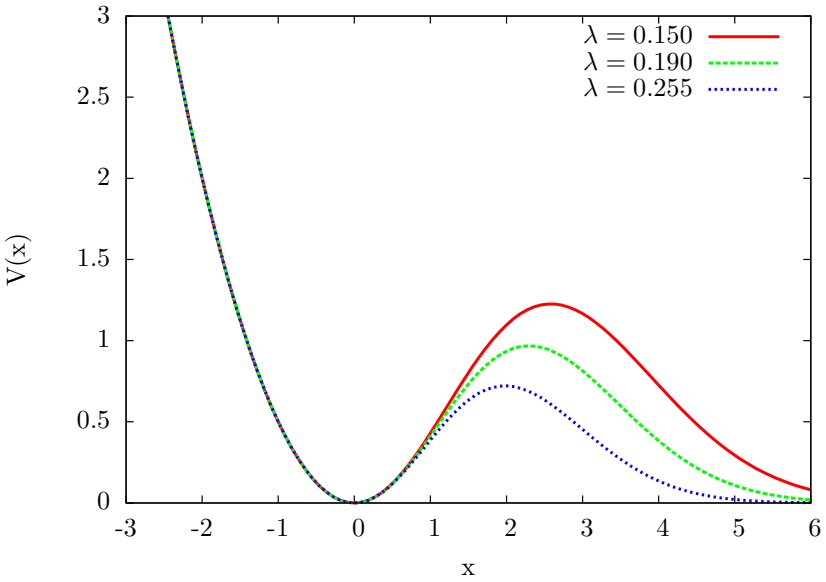

Figure 5.3. *Potential from the Hazi paper, for some different values of the parameter λ.*

By using the basis expansion method for the problem defined by the potential (5.1), one can directly compare the decay rates to the published results [13]. A comparison can be found in Table 5.1. As can be seen from the table, the results are the same to a high precision. It should be noted that our given values are stable with respect to changes of the contour, as long as the contour is never too close to the resonance pole and also not too far. They are also stable with respect to changing the point density on the contour.

The Hazi paper [13] also gives other data than the one shown in Table 5.1, and it has been verified that much of this data can be reproduced by using a harmonic oscillator basis and the same methodology as described in this thesis. The accuracy with which the results obtained using the complex

λ	Parameter	Hazi [13]	Basis Expansion
0.125	E_r	0.472 940	0.472 940
	Γ	$3.607 \cdot 10^{-5}$	$3.649\,860 \cdot 10^{-5}$
0.15	E_r	0.466 105	0.466 105
	Γ	$3.210 \cdot 10^{-4}$	$3.210\,816 \cdot 10^{-4}$
0.19	E_r	0.453 54	0.453 533
	Γ	$2.805 \cdot 10^{-3}$	$2.804\,222 \cdot 10^{-3}$
0.225	E_r	0.441 33	0.441 333
	Γ	$8.996 \cdot 10^{-3}$	$9.002\,093 \cdot 10^{-3}$
0.26	E_r	0.429 03	0.429 033
	Γ	$1.976 \cdot 10^{-2}$	$1.977\,600 \cdot 10^{-2}$

Table 5.1. *Comparision between the exact values of Table IV of [13] and the values obtained by the basis expansion method employed in this project.*

momentum basis concurs with the literature results is a verification of the validity of this approach in one dimension.

5.3 Two Particles in a Harmonic Oscillator Potential

The energy levels for two interacting particles in an infinite-well harmonic-oscillator potential were described in Section 3.12. These were also calculated using the computation routines in this project, as a means of verification. The complex-momentum basis was then replaced by a harmonic-oscillator basis.

In Figure 5.4 the theoretical values (solid lines) as given by (3.25) are compared to the values calculated using a basis expansion of $n = 30$ harmonic-oscillator basis states. Following the convention by [1], the horizontal axis is given not in terms of the coupling coefficient g, but rather in terms of $-1/g$.

As can be seen from the figure, the calculated values closely resembles the theoretical ones, even for strong interaction. For the small deviations of the calculated values using strong interaction, the deviation is always towards larger energies. This is expected, since one can prove that for any trial wavefunction, a variational method will never underestimate the energy.

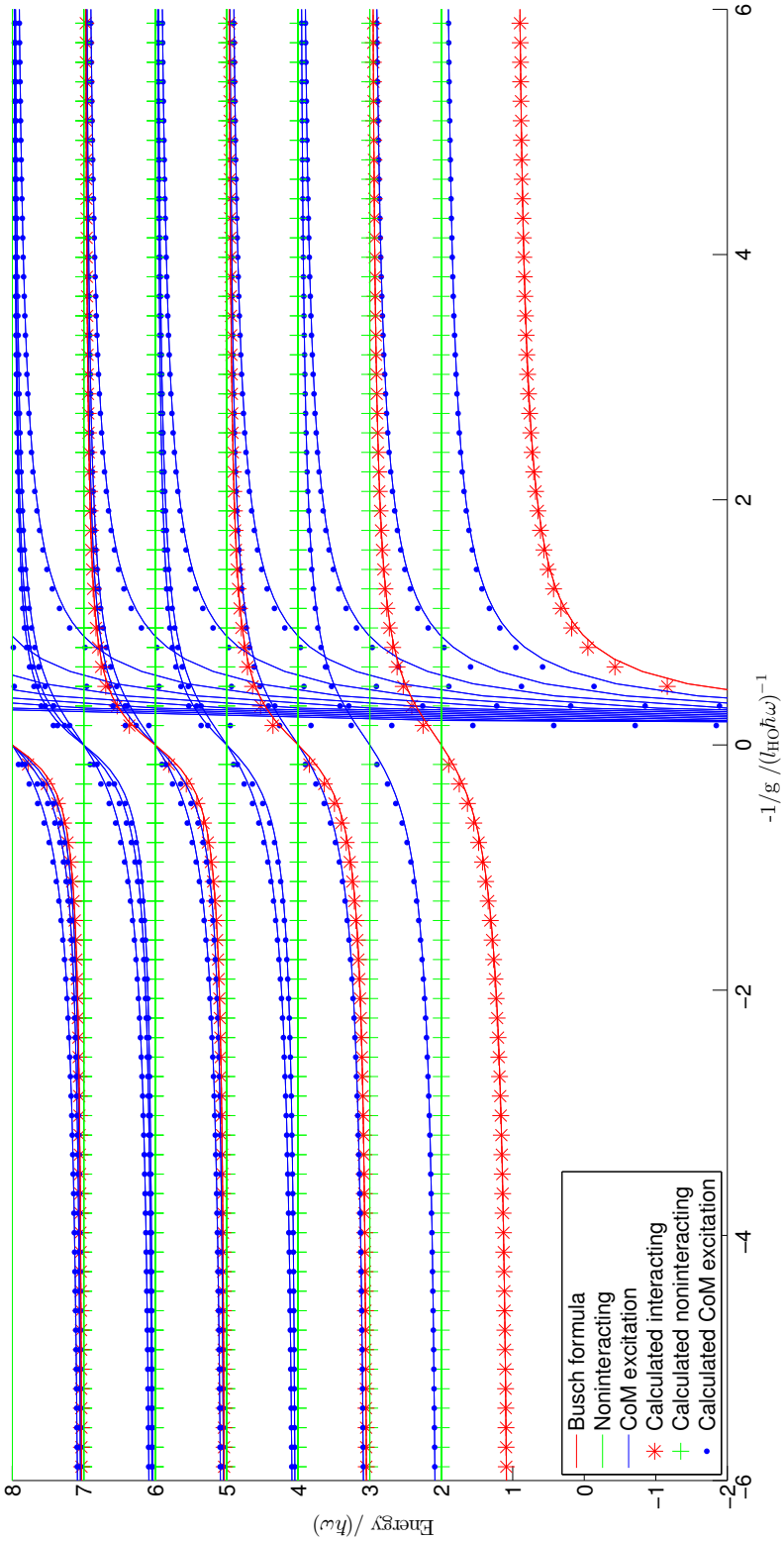

Figure 5.4. *Comparison between the Busch formula (3.25) and the basis expansion method. The solid lines correspond to (exact) theoretical values for interacting and non-interacting systems, respectively. The blue markers correspond to center of mass excitations, as described in the text.*

Chapter 6

Results

The main results of this work are described in this section. First, results and discussions pertaining to one particle in the potential (2.3) are introduced, and some modifications of the fitted potential parameters in this potential are suggested and tested. Thereafter results for two interacting particles are discussed.

6.1 Single-Particle Tunneling

Initially, the potential (2.3) with the parameters from Table 2.2 was used to calculate tunneling rates and energies. The resulting energies and tunneling rates can be found in Table 6.1 for some different values of $c_{B|\text{state}\rangle}$. The results are stable with respect to reasonable changes in the contour L_+ and changes in number of basis states, as long as the number of basis states is large enough.

As can be seen from the table, the calculated energy is within 4 % from a WKB calculation. The tunneling rates however deviate quite a bit from the experimental values. Looking closer at the discussion of the potential in references [2, 3], one can note that some of the parameters, in particular B' and p, are fitted using a WKB calculation together with experimentally measured tunneling rates, rather than measured directly. Since a WKB calculation only yields an approximation, and the outcome of the calculation is very sensitive to those parameters, this may be the reason for the apparent large deviation in tunneling rates.

It should be noted that these tunneling rates correspond to a very small Γ (see Equation (3.5)). The imaginary part of the energy is typically several orders of magnitude smaller than the real part. This requires many basis states on L_+ in order to get the desired accuracy in the results.

The probability densities $|\Psi(z)|^2$ for some resonant states are illustrated in Figure 6.1. Note that the wavefunctions does not quite go to zero at the right limit, since they are not normalizable. If the horizontal axis in

$c_{B\|\mathrm{state}\rangle}$	$E^{\mathrm{calc}}_{B\|\mathrm{state}\rangle}$ /(nK · k_B)	$\gamma^{\mathrm{calc}}_{B\|\mathrm{state}\rangle}$ /(s^{-1})	$E^{\mathrm{new}}_{B\|\mathrm{state}\rangle}$ /(nK · k_B)	$\gamma^{\mathrm{new}}_{B\|\mathrm{state}\rangle}$ /(s^{-1})	$E^{\mathrm{WKB}}_{B\|\mathrm{state}\rangle}$ /(nK · k_B)	$\gamma^{\mathrm{exp}}_{B\|\mathrm{state}\rangle}$	$\sigma^{\mathrm{exp}}_{B\|\mathrm{state}\rangle}$
1.004 57	14.29	56.44	14.84	33.60	-	35.25	3.57
1.004 07	14.33	54.22	14.88	32.17	-	-	-
1.003 56	14.37	52.03	14.92	30.77	-	-	-
1.003 11	14.41	50.16	14.95	29.58	-	30.12	2.81
1.000 00	14.67	38.71	15.19	22.38	15.18	-	-
0.999 68	14.69	37.67	15.22	21.73	-	21.76	1.12
0.998 06	14.82	32.76	15.33	18.71	-	-	-
0.995 12	15.05	25.24	15.54	14.16	-	-	-
0.989 89	15.43	15.53	15.90	8.46	-	8.28	0.49

Table 6.1. *Energies and tunneling rates for a single particle in the trapping potential (2.3) with $c_{B|state\rangle}$ as given by the first column. The second and third column gives our calculated energies E^{calc} and tunneling rates γ^{calc} using the parameters from Table 2.2. The fourth and fifth columns shows our calculated energies E^{new} and tunneling rates γ^{new} using a refined potential, as described in Section 6.2. The seventh column shows the energy E^{WKB} for $c_{B|state\rangle} = 1$ from [5], and the last two columns show the experimental values γ^{exp} from [3], with the standard deviation σ^{exp} also from [3].*

the figure is continued to the right, the wavefunctions would be observed to diverge and behave like e^{ikz} for a complex value of k. The probability densities for the refined potential (see Section 6.2) are very similar to these.

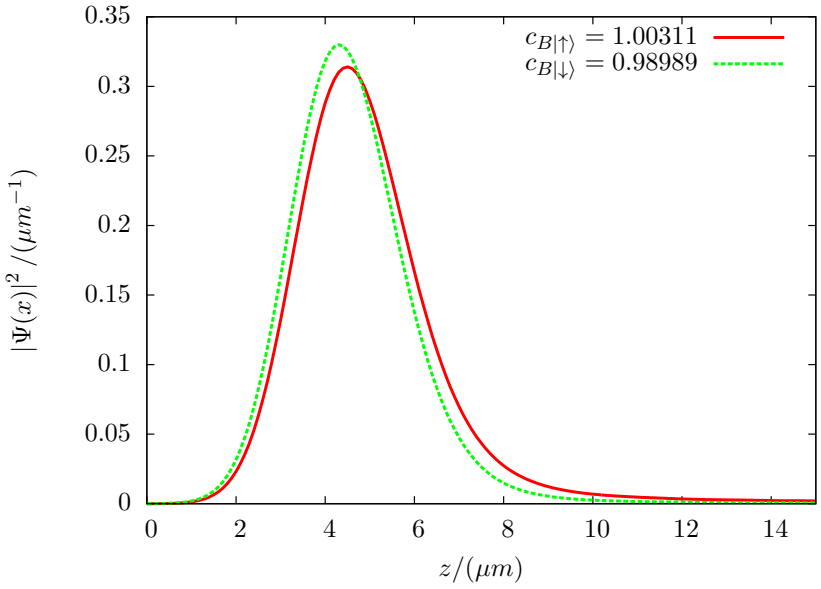

Figure 6.1. *The single-particle probability density* $|\Psi(z)|^2$ *for a particle in the deepest resonant state of the potential, 2.3 with the parameters from Table 2.2, and for some different values of* $c_{B|state\rangle}$.

Figure 6.2 shows a representative example of the eigenstates of the kinetic operator along the contour L_+, and the eigenstates of the full Hamiltonian. From the figure it is clear that the resonance is located away from the contour, distinguishing it from the continuum states.

6.2 Refitting the Trap Potential

The trap parameters B' and p from Table 2.2 were originally fitted to reproduce experimental tunneling rates using a WKB approximation [2]. These parameters may just as well be obtained using our basis expansion method. We fix the other potential parameters in the table except for B' and p, ignoring experimental uncertainties. In particular, any uncertainties in $c_{B|\text{state}\rangle}$ are ignored. The four measured single-particle tunneling rates, including error bars, from Table 6.1 are utilized. We can then define a chi-squared statistic

$$\chi^2(B', p) \equiv \sum_{B|\text{state}\rangle} \left(\frac{\gamma^{\text{calc}}_{B|\text{state}\rangle} - \gamma^{\text{exp}}_{B|\text{state}\rangle}}{\sigma_{\gamma_{B|\text{state}\rangle}}} \right)^2 \tag{6.1}$$

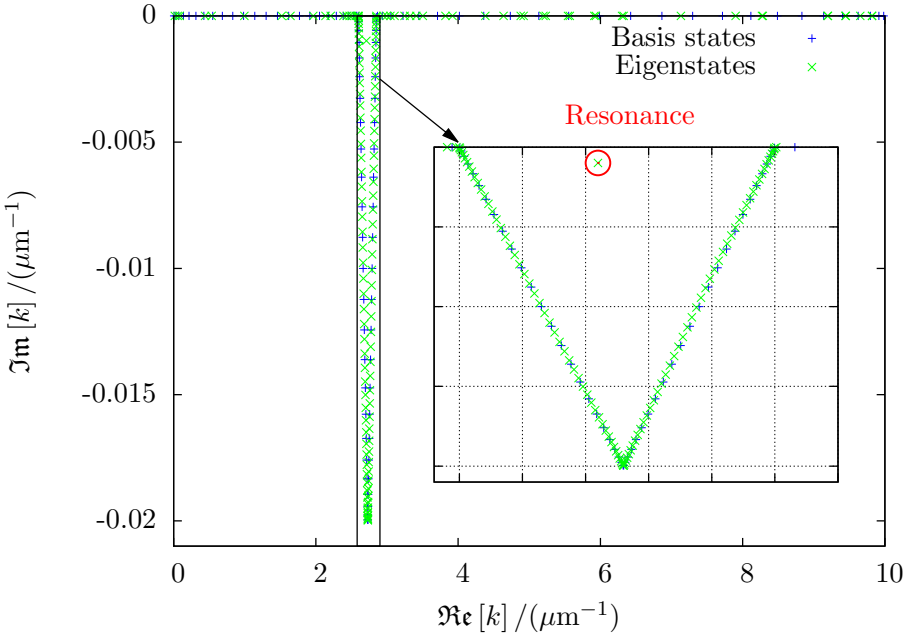

Figure 6.2. *A representative example of the location in momentum space of the basis states and single-particle eigenstates. The area around the most interesting part, the resonance, is magnified.*

and try to minimize its value. Figure 6.3 shows how the value of (6.1) varies over the B'-p parameter plane.

From the figure, it is clear that the local minima form a straight line. In order to choose some potential parameters that fits the data, a point on this straight line must be chosen. Arbitrarily the closest point to [3], which is given by the orthogonal projection of that point onto the straight line, is chosen. This new point, denoted by λ_{new}, is given by the parameters

$$\begin{cases} B' = 18.92 \cdot 10^{-8}\mathrm{T}/\mu\mathrm{m} \\ p = 0.638\,83 \end{cases}$$

and the function value at this point is $\chi^2(B', p) \approx 0.384$. The values for the energies and tunneling rates with the modified version of the potential are shown in Table 6.1. As can be seen, the calculated tunneling rates are all well within the errors of the experimentally measured values.

6.3 Approximations and Errors

Since the potential used in our calculations is not exactly the one described by [3] (see Section 4.3), it is important to analyze how the choice of cutoff

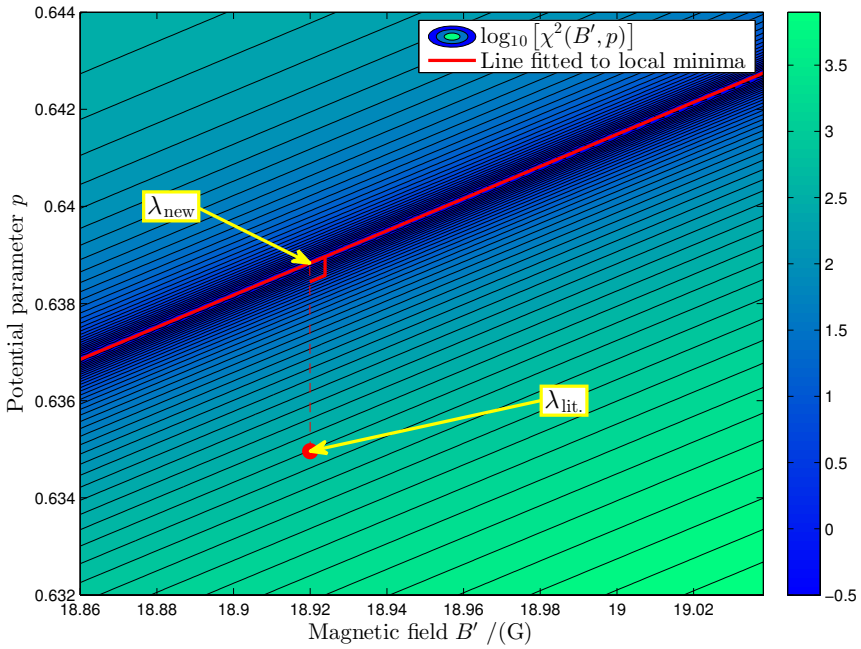

Figure 6.3. *The 10-logarithm of $\chi^2(B',p)$ as defined by Equation (6.1). (B',p) given by [3], as described in Section 2.2, is marked by $\lambda_{\text{lit.}}$ in the Figure. Also marked are local minima, which form a straight line. The orthogonal projection of $\lambda_{\text{lit.}}$ onto this line, denoted λ_{new}, is also marked. This λ_{new} was used in the refined potential.*

parameters a and R_0 in Equation (4.1) affects the result. For changes in a, essentially no change in the resulting complex energies was observed. For changes in R_0, there were small but noticeable fluctuations in the energies and tunneling rates. A small dependence on R_0 is expected, since the potential is indeed modified when R_0 is changed. The relative deviation from the mean value for different values of R_0 is shown in Figure 6.4.

As can be seen from the figure, the fluctuations when lifting the bottom of the potential (increasing R_0) seems to be periodical in R_0. Furthermore, the relative fluctuations for the energy are much smaller than the relative fluctuations for the tunneling rates. Both of them decrease with the lifting of the potential.

Notable is also that the relative magnitude of the fluctuations in the tunneling rates seems to be largely independent on the trap parameter $c_{B|\text{state}\rangle}$.

6.4 Two-Particle Tunneling

If the two particles in the trap would populate the same hyperfine state, they would behave like identical fermions and follow the Pauli principle. Since

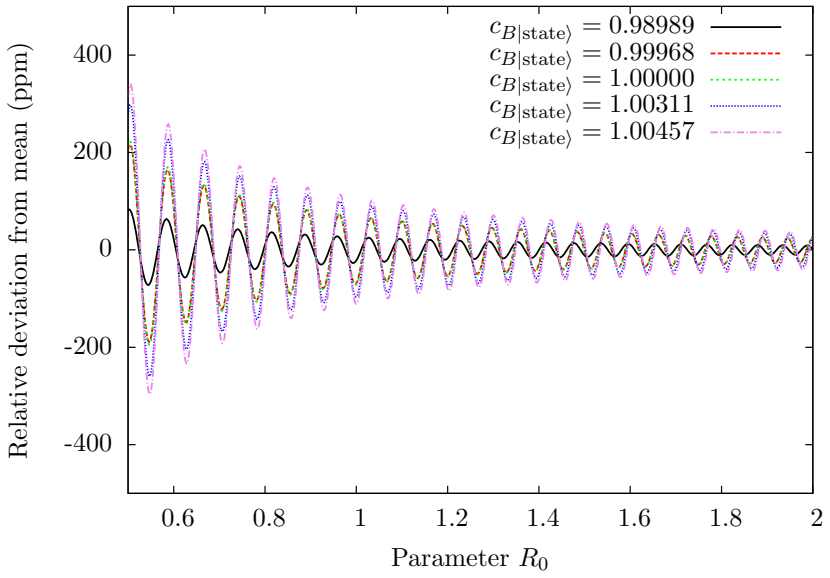

(a)

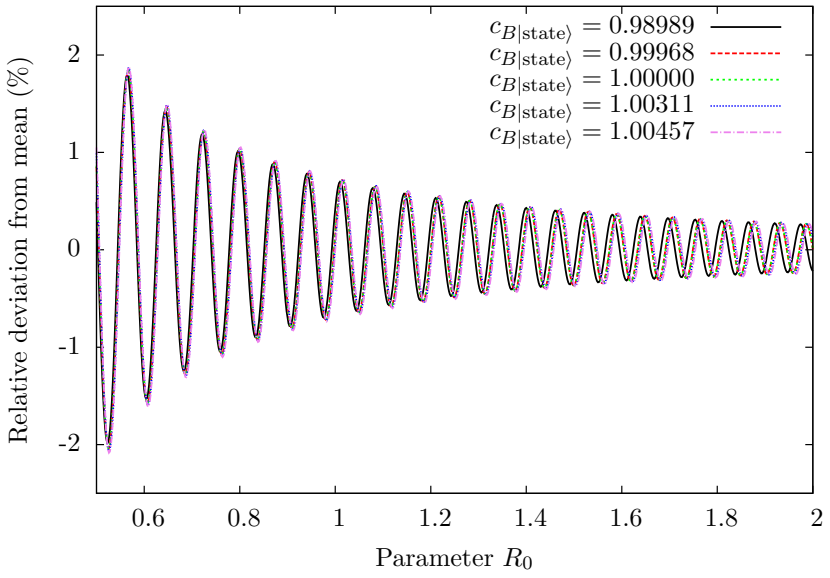

(b)

Figure 6.4. *Relative difference in (a) energies and (b) tunneling rates for different values of the offset R_0 in the regularized potential* (4.1) *using the parameters from Table 2.2.*

the trap is only deep enough to harbor the lowest resonant state of a particle species, this is not the relevant situation for our studies. Furthermore, if the trap was deeper, identical particles would still not interact with each other through a Feshbach resonance. Focus will therefore exclusively be on the case where the two particles are in different hyperfine states and therefore behave like distinguishable particles.

For a given value of the perpendicular magnetic field, the coupling coefficient g as well as $c_{B|\uparrow\rangle}$ and $c_{B|\downarrow\rangle}$ take on well-defined values. Therefore, there is a relation between $c_{B|\uparrow\rangle}$ and $c_{B|\downarrow\rangle}$, which is given by [3]. This is shown in Table 6.2.

$\boldsymbol{g}$	$-0.703\,85$	$-30.969\,33$	$-41.527\,05$	$-45.046\,30$	other [1]
$\boldsymbol{c_{B\|\uparrow\rangle}}$	1.00457	1.00407	1.00356	1.00311	1.00457 [1]
$\boldsymbol{c_{B\|\downarrow\rangle}}$	0.99968	0.99806	0.99512	0.98989	1.00457[1]

Table 6.2. *Relation between g, $c_{B|\uparrow\rangle}$ and $c_{B|\downarrow\rangle}$ values, as given by [3]. g is given in units of* $\mathrm{nK}\cdot\mathrm{k_B}\cdot\mu\mathrm{m}$.

A choice of corresponding g and $c_{B|\mathrm{state}\rangle}$-values is made, and the modified potential parameters from Section 6.2 are used. Thereafter, the two-particle problem is constructed and solved using the choice of potential parameters from Section 6.2.

Resulting tunneling rates and energies of the two-particle states $|\uparrow\downarrow\rangle$ are shown in Table 6.3. The interaction energies, defined as the difference in energy between the interacting and corresponding non-interacting system, are also shown in Figure 6.5. The tunneling rates are available in Figure 6.6. For these calculations, $n_{\max}$ was taken to be 30, with 200 single-particle basis states on a contour L_+. The accuracy of the calculated results will be discussed in the next section.

From the table one can observe a pattern of increasingly negative interaction energies and, to some extent, tunneling rates with an increasingly attractive interaction. This is also what is expected since the effective tunneling barrier is larger. However, for stronger interactions this pattern is not so clear for tunneling rates. In the next section the error in the tunneling rate will be estimated to be in the order of at least a few seconds, and these small tunneling rates are therefore too small to have any significance. That a stronger interaction gives more interaction energy is however clear, and expected.

The tunneling rates and energies differ quite a bit from the values given by [3]. A possible explanation for this is that the WKB approximation

[1] For strong enough magnetic fields, given by [3] as $> 850\,\mathrm{G}$, both $c_{B|\mathrm{state}\rangle}$ are assumed to be the same and equal to 1.00457.

g $/(\mathrm{nK}\cdot\mathrm{k_B}\cdot\mu\mathrm{m})$	$E_{\mathrm{int}}^{\mathrm{calc}}$ $/(\mathrm{nK}\cdot\mathrm{k_B})$	$\gamma_{\mathrm{total}}^{\mathrm{calc}}$ $/(\mathrm{s}^{-1})$	$E_{\mathrm{int}}^{\mathrm{WKB}}$ $/(\mathrm{nK}\cdot\mathrm{k_B})$	$\gamma_{\mathrm{total}}^{\mathrm{exp}}$ $/(\mathrm{s}^{-1})$
−30.969 33	−8.45	19.19	-3.093 ± 0.228	22.20 ± 1.0
−41.527 05	−12.10	12.54	-4.167 ± 0.391	13.84 ± 1.0
−45.046 30	−13.59	25.81	-4.753 ± 0.326	9.70 ± 0.3
−99.946 47	−37.02	(0.44)	(-10.418 ± 1.107)	2.14 ± 0.2
−104.169 56	−39.28	(0.56)	(-10.646 ± 0.912)	1.93 ± 0.1
−110.504 19	−42.79	(1.12)	(-11.623 ± 0.814)	1.23 ± 0.1
−123.877 31	−50.55	(0.34)	(-13.283 ± 0.977)	0.51 ± 0.0

Table 6.3. *Energies and tunneling rates for two interacting particles with different coupling coefficients g as given by the first column, in the trapping potential (2.3) with the corresponding $c_{B|state\rangle}$ pairs as in Table 6.2. The second column E_{int}^{calc} corresponds to the calculated interaction energy, which is defined as the energy for the interacting resonant state minus the energy for both particles in the resonant state without interaction. The third column γ_{total}^{calc} corresponds to the sum of tunneling rates through all channels, as explained in Section 2.3. The fourth column E_{int}^{WKB} corresponds to results from [3]. The errors in the second and third column have a lower bound estimated in Section 6.4.1, while the error in the fourth column is given by [3]. The parenthesis on values in the third column are used to mark insignificant values compared to the error estimate. The parenthesis on some of the values in the fourth column are given by [3], and indicate large systematic errors.*

(see Appendix D) used to derive potential parameters may be insufficient to describe tunneling in this case. Furthermore, the choice of new potential parameters in Section 6.2 was not unique, and it is possible that another choice would have given results that more closely resembles the values in reference [3].

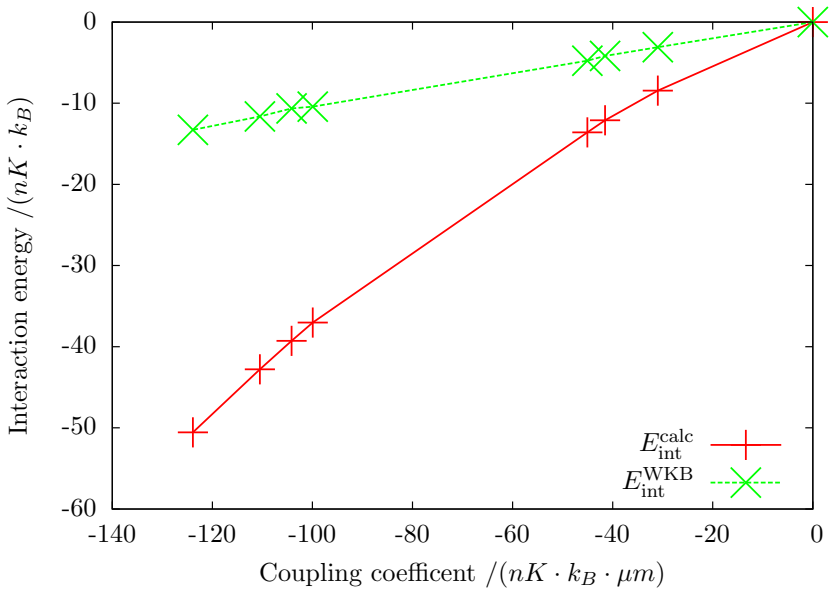

Figure 6.5. *Interaction energies calculated by the basis expansion method, and the interaction energies given by [3].*

An attentive reader may have noted that the tunneling rate for the coupling coefficient $g = -45.046\,30\text{nK} \cdot \text{k}_\text{B} \cdot \mu\text{m}$ in Table 6.3 is higher than for the coupling coefficients closer to zero. This is likely due to the fact that slightly different single-particle potentials were used, as discussed above. For an example on how the shape of the potential affects the results, assume that the potential corresponding to $g = -30.969\,33\text{nK} \cdot \text{k}_\text{B} \cdot \mu\text{m}$ were to be used in conjunction with the coupling coefficient $g = -45.046\,30\text{nK} \cdot \text{k}_\text{B} \cdot \mu\text{m}$. The calculated interaction energy then becomes $-13.21\text{nK} \cdot \text{k}_\text{B}$, with a tunneling rate 14.51s^{-1}. Thus, given the same single-particle potentials, the tunneling rate is decreasing with increasing interaction strength, as expected.

6.4.1 Stability of Results

The stability of the value of the energy with respect to different parameters may be investigated in order to assess the accuracy of the results.

Figure 6.7 shows the interaction energy and tunneling rate as a function of the cutoff level n_max for a given contour L_+ in Equation (3.19). As can be seen, the relative changes in energy when increasing the number of points

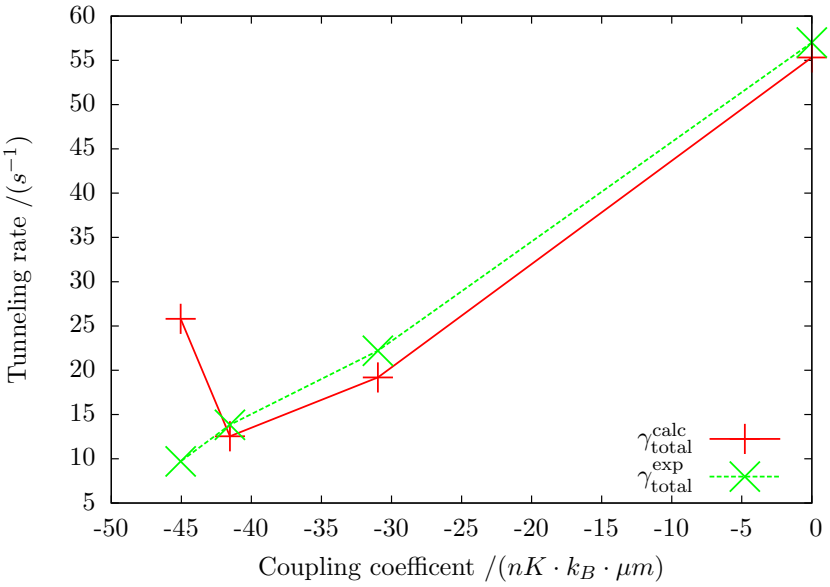

Figure 6.6. *Tunneling rates calculated by the basis expansion method, and experimental values given by [3].*

on the contour is small. The relative change in tunneling rate is larger, but still (for the larger values of $n_{\max}$) more than an order of magnitude smaller than unity. Also, the energy is decreasing with increasing $n_{\max}$, which is intuitively expected for a variational-calculation theory. Using more states on the contour L_+, which is discussed below, might increase the convergence rate with respect to $n_{\max}$.

Figure 6.8 shows the interaction energy and tunneling rate as a function of the number of basis states on a specific contour L_+. As is clear from the figure, the relative difference in energy when increasing the number of states is not very large. However, the difference in tunneling rate is for this case larger than $1\,\mathrm{s}^{-1}$. The order of magnitude for the differences is the same as for the $n_{\max}$-dependence in Figure 6.7.

Figure 6.9 shows the interaction energy and tunneling rate for different contours L_+. Since the resonance is physical, it is expected to be independent on the choice of contour. However, from the figure it is clear that the contour-dependence is of the same order of magnitude as the $n_{\max}$ and basis-size dependence shown in Figure 6.7 and 6.8. A reasonable explanation for this contour dependence is that the number of basis states along the contour needs to be larger to achieve a more stable resonance, as was concluded above.

The larger deviations in the tunneling rates compared to the interaction energies shown in this section are most likely due to the fact that the imaginary part of the energy is several orders of magnitude smaller than the

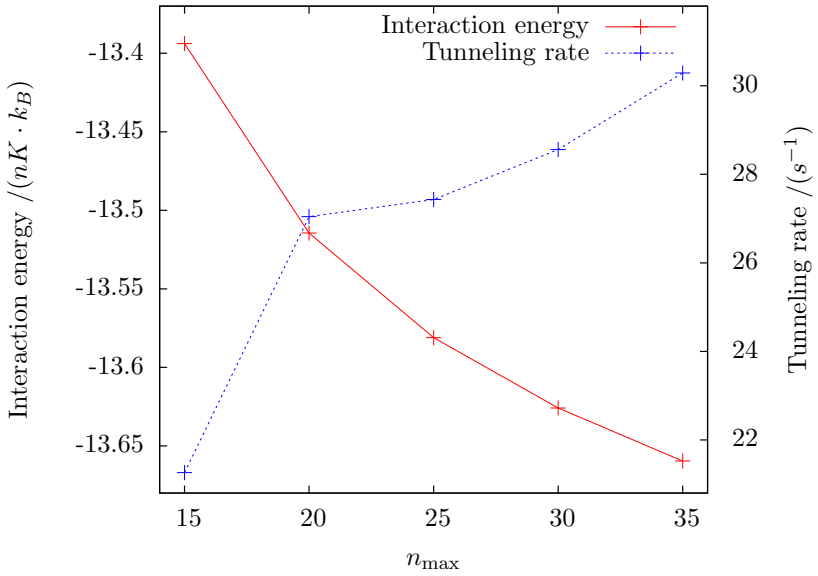

Figure 6.7. *Interaction energy and tunneling rate as a function of the cutoff level n_{max} in the sum in Equation* (3.19)*, for a specific contour.*

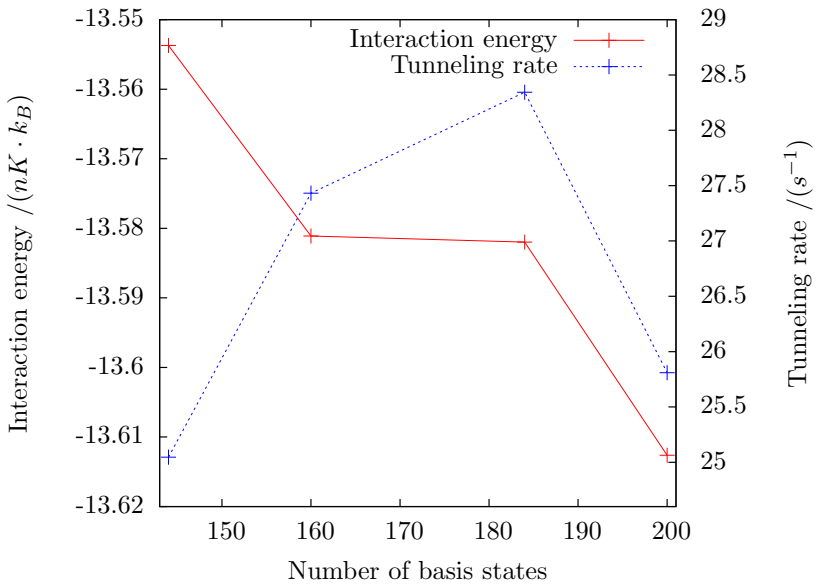

Figure 6.8. *Interaction energy and tunneling rate as a function of the number of single-particle basis states used, using a specific contour L_+ consisting of four segments with equal number of points on each segment.*

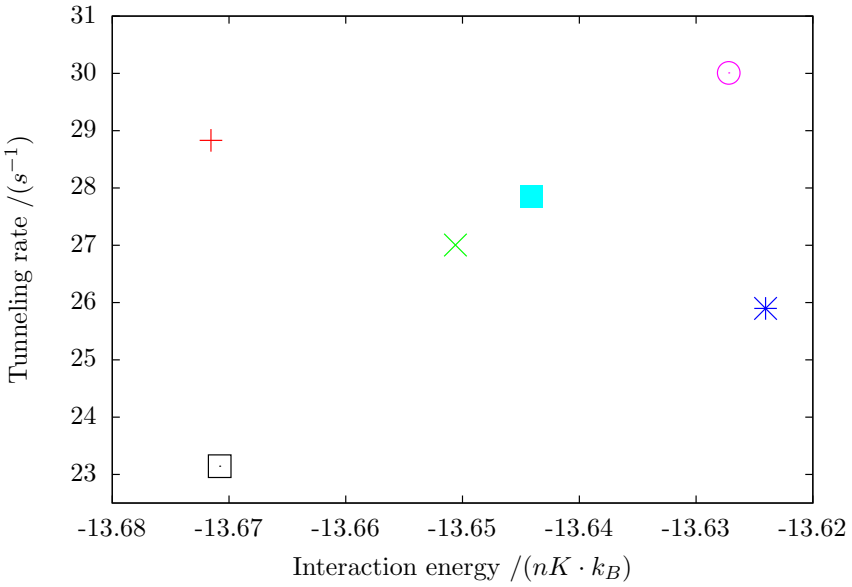

Figure 6.9. *Interaction energy and tunneling rate for six different contours L_+, each with 200 single-particle basis states, using the same coupling coefficient and a cutoff level $n_{max} = 30$.*

real part. This means that in order to get accurate results for the tunneling rates, an even more accurate result for the modulus of the energy is needed.

This is also the reason that perturbation theory as mentioned in Section 3.13 is not relied upon to obtain the energies and tunneling rates. A perturbative expansion was done to the third order as in Equation (3.26), for the same contour L_+ as in Figure 6.7, with $n_{\max} = 25$ and 160 points on the contour. This gave the correct first four significant digits of the modulus of the energy. However, the error in the tunneling rate compared to the value obtained by exact diagonalization was about 50%. Finding the eigenvalues requires less computational work than evaluating the perturbative expansion further than the third order.

It is hard to make any conclusive error estimates based on the results in this section. The tunneling rates are observed to vary by a few inverse seconds for different choices of parameters, and the interaction energies by one or a few tenths of a nK. These estimates can therefore be taken as a lower bound on the error.

Chapter 7

Conclusion and Outlook

In this work, tunneling of one and two interacting distinguishable fermions out of a one-dimensional trap has been studied using a basis-expansion method. The method was verified by comparing it to results obtained by other methods and studies.

The general method for a one-dimensional potential was applied to a specific trapped atomic system, which has been studied both experimentally [1, 2, 3] and theoretically [4, 5]. The energies and tunneling rates calculated by the basis expansion method were compared to the results of these previous studies, and discrepancies were found. These discrepancies could possibly be explained by experimental error margin and/or the WKB approximation used to supplement the experimental data in deriving the potential parameters.

An issue, especially in the two-fermion case, has been the large computational resources required to perform the calculations, both in terms of memory and CPU time. The practical consequence of this has been limited statistics in terms of different parameters such as the path of the contour L_+ in the complex plane, the interaction cutoff $n_{\max}$ and the number of basis states on L_+.

Interesting physics can be investigated in future projects by adding more particles to the trap. In particular, it may be possible to study correlations and shell effects can be in a high-fidelity environment. Such systems have already been studied experimentally [1] and so a theoretical explanation of these results, built on the same principles as this work, may be of much interest. This will lead to much larger, but sparse, matrices. Practically this means that many eigenvalue algorithms would be problematic to use. For example, both QR iteration and a shift-inverted Arnoldi algorithm would destroy the sparsity of the matrix. A method that might resolve this issue is Jacobi rotations [14, p. 192].

It would also be interesting to use the basis expansion method for stronger interactions than covered here. This might require some way of handling

strong correlations, in particular to reduce the number of basis states required to reach convergence. For instance, one may use a unitary transformation to accomplish this [15, 16]. It is also possible that such a transformation would increase the accuracy for very small tunneling rates encountered with attractive interactions.

Furthermore, it would likely be possible to demonstrate fermonization in a similar (but deeper) trap using the methods described in this thesis. This is the limit of strong repulsive interaction between distinguishable fermions, and can be seen as an "effective" Pauli principle. The fermions then tend to avoid each other [17], just as two identical fermions would do. The energy and modulus square of the wavefunction will then be similar to the case of two identical fermions in the trap.

Making the inter-particle interaction repulsive should move the states closer to the trap barrier and increase the tunneling rate, which would increase the relative accuracy in the calculations since it would mean that the imaginary part of the energy becomes larger. Future experiments may also provide data to compare with such theoretical results.

References

[1] G. Zürn. Few-fermion systems in one dimension, 2012.

[2] G. Zürn, F. Serwane, T. Lompe, A. N. Wenz, M. G. Ries, J. E. Bohn, and S. Jochim. Fermionization of two distinguishable fermions. *Physical review letters*, 108(7):075303, 2012.

[3] G. Zürn, A. N. Wenz, S. Murmann, A. Bergschneider, T. Lompe, and S. Jochim. Pairing in few-fermion systems with attractive interactions. *Physical review letters*, 111(17):175302, 2013.

[4] M. Rontani. Tunneling theory of two interacting atoms in a trap. *Physical review letters*, 108(11):115302, 2012.

[5] M. Rontani. Pair tunneling of two atoms out of a trap. *Physical Review A*, 88(4):043633, 2013.

[6] J. Bengtsson, P. Granström, O. Embréus, V. Ericsson, and N. Wireklint. Quantum resonances in a complex-momentum basis, 2013. 59.

[7] Z. X. Xu, R. J. Liotta, C. Qi, T. Roger, P. Roussel-Chomaz, H. Savajols, and R. Wyss. Calculation of the spectrum of 12li by using the multistep shell model method in the complex energy plane. *arXiv preprint arXiv:1004.4083*, 2010.

[8] J. J. Sakurai and J. Napolitano. *Modern Quantum Mechanics*. International edition. Addison-Wesley, 2011.

[9] A. I. Baz, Y. B. Zeldovich, and A. M. Perelomov. *Scattering, reactions and decay in nonrelativistic quantum mechanics*. Jerusalem, 1969.

[10] T. Berggren. On the use of resonant states in eigenfunction expansions of scattering and reaction amplitudes. *Nuclear Physics A*, 109(2):265–287, 1968.

[11] T. Busch, B. G. Englert, K. Rzażewski, and M. Wilkens. Two cold atoms in a harmonic trap. *Foundations of Physics*, 28(4):549–559, 1998.

[12] C. Buth, R. Santra, and L. S. Cederbaum. Non-hermitian rayleigh-schrödinger perturbation theory. *Physical Review A*, 69(3):032505, 2004.

[13] A. U. Hazi and H. S. Taylor. Stabilization method of calculating resonance energies: Model problem. *Phys. Rev. A*, 1:1109–1120, Apr 1970.

[14] M. T. Heath. *Scientific computing: an introductory survey*. McGraw-Hill Higher Education. McGraw-Hill, 2002.

[15] J. Rotureau. Interaction for the trapped fermi gas from a unitary transformation of the exact two-body spectrum. *The European Physical Journal D*, 67(7):1–9, 2013.

[16] J. Lindgren. Fermionization in one-dimensional cold atom systems. Master's thesis, Chalmers University of Technology, 2013. 65.

[17] F. Deuretzbacher, K. Fredenhagen, D. Becker, K. Bongs, K. Sengstock, and D. Pfannkuche. Exact solution of strongly interacting quasi-one-dimensional spinor bose gases. *Physical review letters*, 100(16):160405, 2008.

[18] J. Stoer and R. Bulirsch. *Introduction to numerical analysis*, volume 12. Springer, 2002.

[19] M. Abramowitz and I. A. Stegun. *Handbook of mathematical functions: with formulas, graphs, and mathematical tables*. Dover Publications, 1964.

[20] P. Hansson, J. Löfgren, K. S. Keiding, and S. Vajedi. Configuration interaction methods and large-scale matrix diagonalization, 2012. 118.

[21] M. Schatzman. A simple proof of convergence of the qr algorithm for normal matrices without shifts. *IMA Preprint Series*, 720, 1990.

[22] J. W. Demmel. *Applied numerical linear algebra*. Siam, 1997.

[23] C. Chin, R. Grimm, P. Julienne, and E. Tiesinga. Feshbach resonances in ultracold gases. *Reviews of Modern Physics*, 82(2):1225, 2010.

[24] D. J. Griffiths. *Introduction to Quantum mechanics. 2005*. Pearson Prentice Hall, NJ, 2004.

Personal Communication

[25] J. Rotureau. (2014-02-18) Software obtained by personal communication (SSH).

Glossary

Attractive interaction In this thesis, a point-interaction with a coupling coefficient $g < 0$.

BCS Theory of superconductivity in which electrons pair up to so-called Cooper pairs.

Condition number Given a square matrix A, the condition number is defined as $\text{cond}(A) \equiv ||A|| \cdot \left|\left|A^{-1}\right|\right|$ if A is nonsingular, and $\text{cond}(A) \equiv \infty$ if A is singular.

Coupling coefficient The quantity g in Equation (3.17), which is controlled by a Feshbach resonance.

Decay rate Same thing as *tunneling rate* in the context of this thesis.

Harmonic oscillator units Units in which length and energy are expressed using a reference frequency, see Section 1.3.2.

Feshbach resonance Feature of many-body system with which the interaction strength between atoms can be controlled by changing a magnetic field, see Appendix C.

Interaction energy The difference in energy between an interacting and a non-interacting system of particles.

Interaction strength Strength of inter-particle interaction, characterized by the modulus of the coupling coefficient.

Matrix size The number of rows or columns of a square matrix.

Molecular units Unit system with the energy expressed in $\mu K \cdot k_B$, the time in μs and length in μm. See Section 1.3.1.

Pole In this thesis, pole refers to a pole of the S-matrix if nothing else is stated.

Repulsive interaction In this thesis, a point-interaction with a coupling coefficient $g > 0$.

S-matrix A matrix relating initial and final states in a scattering process.

Stationary state A state with a single definite energy, where the probability density is independent of time.

Tunneling rate In this thesis, the rate by which atom(s) tunnel out of a certain region in a trap.

Ultracold atom Atom at a temperature close to 0 K, typically in the order of μK or nK.

Weak interaction Interaction in which the interaction energy is small compared to the spacing of the single-particle energy levels.

WKB approximation Popular approximation method in quantum mechanics, see Appendix D.

Appendix A

Numerical Quadrature

A so-called *quadrature rule* is an approximation of the definite integral of a function. Consider the integral

$$I[f] = \int_a^b \mathrm{d}x \omega(x) f(x) \tag{A.1}$$

where ω is a weight on $[a, b]$, such that $\int_a^b \mathrm{d}x x^k \omega(x)$ exists and is finite, $\forall k \in \mathbb{Z}^+$, and for all polynomials $p(x)$ which are nonnegative on $[a, b]$,

$$\int_a^b \mathrm{d}x \omega(x) p(x) = 0 \implies p(x) = 0.$$

Also, a and/or b may be infinite.

This integral (A.1) can then be approximated by a sum,

$$I(f) \approx \sum_{i=1}^{N} w_i f(x_i) \tag{A.2}$$

where $\{w_i\}_{i=1}^N$ are weights for the corresponding points $\{x_i\}_{i=1}^N$.

The *order* of a quadrature rule rule is defined as the maximum degree of polynomials such that all polynomials with this degree are integrated exactly. For a given weight function $w(x)$, interval $[a, b]$ and number of points N it can be shown that there is a unique way of choosing the points and weights such that the order becomes maximal, and that this maximal order is $2N-1$. Furthermore, for this optimal choice, $w_i > 0$ and $a < x_i < b$. Such a quadrature rule is called a *gaussian quadrature* [18, p. 171-181].

In this thesis, two specializations of the gaussian quadrature are used, Gauss-Legendre quadrature and Gauss-Hermite quadrature.

A.1 Gauss-Legendre quadrature

For the case of $\omega(x) = 1$ and $[a, b] = [-1, 1]$, the optimal quadrature rule (A.2) is known as a Gauss-Legendre quadrature. The x_i's are chosen as zeros

for the N:th order Legendre polynomials $P_n(x)$ and the w_i's are chosen as [19, p. 887]

$$w_i = \frac{2}{\left(1 - x_i^2\right)\left[P_n'(x_i)\right]^2}$$

For an integral over an interval $[a, b] \neq [-1, 1]$ (but still finite) with and $\omega(x) = 1$ it is easy to see that the rule can be rescaled by a simple change of variables.

A.2 Gauss-Hermite Quadrature

For the case of $\omega(x) = e^{-\beta(x-\alpha)^2}$ with $a = -\infty$ and $b = \infty$, the optimal quadrature rule is called a Gauss-Hermite rule, and another choice of coefficients and weights than for the Gauss-Legendre rule is made. It is easy to see that the weight function can be rewritten on so-called standard form $\omega(x) = e^{-x^2}$ by a change of variables.

Using the standard form of the weight function, the x_i:s are chosen as zeroes for the N:th order Physicist's Hermite polynomials (3.14), and the weights w_i are chosen as [19, p. 890]

$$w_i = \frac{2^{n-1} n! \sqrt{\pi}}{n^2 \left[H_{n-1}(x_i)\right]^2}.$$

In some calculations in this thesis, the weight function is on the form $\omega(x) = e^{-\beta_1(x-\alpha_1)^2} e^{-\beta_2(x-\alpha_2)^2}$. This can be rewritten by expansion and square completion in the exponent. We then get

$$\beta_1(x-\alpha_1)^2 - \beta_2(x-\alpha_2)^2 = \tilde{b}\,(x-\tilde{a})^2 - R$$

where

$$\begin{cases} \tilde{b} & \equiv \beta_1 + \beta_2 \\ \tilde{a} & \equiv \frac{\beta_1\alpha_1 + \beta_2\alpha_2}{\beta_1 + \beta_2} \\ R & \equiv \frac{\beta_1\beta_2}{\beta_1+\beta_2}\,(\alpha_1 - \alpha_2)^2 \end{cases}$$

and thus the weight function can be written as $e^{-R} e^{-\tilde{b}(x-\tilde{a})^2}$ which enables us to use the Gauss-Hermite quadrature rule.

Appendix B

Numerical Eigenvalue Methods

An essential computational problem in this project is to find eigenvalues of large, dense matrices. There are several different approaches in doing this, and two different concepts have been employed: QR iteration and Krylov subspace methods. The Krylov subspace methods frequently use QR iteration as a part of the algorithm.

In this appendix a brief overview of these two methods is presented, in large based on [14, 20] where a more thorough description can be found.

B.1 QR Iteration

QR iteration is a process that can reduce a general matrix A to a triangular matrix T, the so-called *Schur form* of A, through similarity transforms. Since two similar matrices have the same eigenvalues, the diagonal entries in T must be the eigenvalues of A.

If A is an $n \times n$ matrix, then it can be factored as a product of two matrices, $A = QR$ where Q is a unitary matrix and R is an upper triangular matrix. This is the so-called *QR factorization* of A.

The main idea used to accomplish the similarity transform from A to T is to employ repeated QR factorization and multiplying the matrices Q and R back together in the reverse order. To see this, let $A_k = Q_k R_k$ be a QR-factorization of the matrix A_k, and let $A_{k+1} = R_k Q_k$. Then $R_k = Q_k^{-1} A_k$ and thus

$$A_{k+1} = Q_k^{-1} A_k Q_k$$

which is a similarity transformation. Also, since Q_k is unitary, $Q_k^{-1} = Q_k^{\dagger}$. A proof that the general QR algorithm with shifts converge to a triangular matrix can be very complicated [21] and will not be covered here.

In practice, there are multiple other considerations that needs to be taken into account. For example, the matrix may converge towards the eigenvalues faster if it is shifted by a multiple of the identity matrix before computing the QR factorization. Also, the algorithm can be made much more efficient by initially performing a similarity tranform to an *upper Heisenberg* matrix (a matrix with zeroes below the first subdiagonal). An interested reader may find more information on improving the QR iteration efficiency in [22, pp. 159-173].

For a general purpose QR algorithm, the `LAPACK` routine `ZGEEV` (see Appendix E) has been used.

B.2 Krylov Subspace Methods

Two similar so-called Krylov subspace methods have been used in this project, the *Arnoldi algorithm* and the *Lanczos algorithm*. The general idea is to find a few of the largest eigenvalues of a matrix, without having to compute all eigenvalues and without having to perform other matrix operations than a matrix-vector product.

For a general $n \times n$ matrix A and an arbitrary starting vector $\boldsymbol{x}_0$, the sequence $\left\{A^k \boldsymbol{x}_0\right\}_{k=0}^{m-1}$ is called a *Krylov sequence*, and we can define a *Krylov matrix* with the elements of this sequence as columns:

$$K_m = \begin{bmatrix} \boldsymbol{x}_0 & A\boldsymbol{x}_0 & \cdots & A^{m-1}\boldsymbol{x}_0 \end{bmatrix} \tag{B.1}$$

The columns can be shown to be linearly independent if m is less than or equal to the number of distinct eigenvalues of A. K_m has a corresponding so-called Krylov subspace $\kappa_m = \text{span}(K_m)$, which gives the name to this class of eigenvalue methods.

Looking at the case $m = n$ and assuming that K_n is nonsingular, A is similar to an upper Hessenberg matrix C_n by $AK_n = K_n C_n$, which can be seen by computing the right hand side (using (B.1)) and left-multiplying the result by the identity $K_n K_n^{-1}$.

The basis of the Krylov subspace κ_m consisting of the columns of K_m becomes increasingly ill-conditioned with increasing m, since the matrix-vector product $A^j \boldsymbol{x}_0$ will grow more in the direction of the dominant eigenvector of A. To fix this, K_n is QR-factorized, $K_n = Q_n R_n$, which enables us to rewrite the similarity relation for A to

$$AQ_n = Q_n H \tag{B.2}$$

with H as another upper Hessenberg matrix similar to C_n by $H \equiv R_n C_n R_n^{-1}$.

If $Q_n = \begin{bmatrix} \boldsymbol{q}_1 & \boldsymbol{q}_2 & \cdots & \boldsymbol{q}_n \end{bmatrix}$, and the elements of H are denoted $\{h_{ij}\}_{i,j=1}^{n}$, then looking at the k:th column of the similarity equation (B.2) gives

$$A\boldsymbol{q}_k = \sum_{i=1}^{k+1} h_{ik}\boldsymbol{q}_i \tag{B.3}$$

and due to orthogonality this means that

$$\boldsymbol{q}_j^\dagger A \boldsymbol{q}_k = h_{jk}$$

which means that $\boldsymbol{q}_{k+1}$ can be obtained from the first k $\boldsymbol{q}_i$-vectors through one matrix-vector multiplication by using (B.3).

Now partition $Q_n = \begin{bmatrix} Q_k & U_k \end{bmatrix}$ where Q_k contains the first k columns of Q_n and U_k the remaining $(n-k)$ columns. Assume that Q_k is calculated using the method above, while U_k is unknown. The similarity relation (B.2) can then be written

$$H = Q_n^\dagger A Q_n = \begin{bmatrix} Q_k^\dagger \\ U_k^\dagger \end{bmatrix} A \begin{bmatrix} Q_k & U_k \end{bmatrix} = \begin{bmatrix} Q_k^\dagger A Q_k & Q_k^\dagger A U_k \\ U_k^\dagger A Q_k & U_k^\dagger A U_k \end{bmatrix} = \begin{bmatrix} H_k & M \\ \tilde{H}_k & N \end{bmatrix}$$

Obviously, H_k can then be calculated, while M and N can not. $\tilde{H}_k$ only contains one nonzero element, since H is upper Hessenberg. The eigenvalues of H_k are so-called *Ritz values*, and the vectors $Q_k\boldsymbol{y}$ (where $\boldsymbol{y}$ is an eigenvector of H_k) are called *Ritz vectors*. It can be shown that the Ritz values and Ritz vectors converge towards eigenvalues and eigenvectors of A, respectively, with increasing k. The eigenvalues and eigenvectors of H_k can be calculated using QR iteration, as described above, which hopefully requires much less work than performing QR iteration on A if $k \ll n$.

The method described for finding eigenvalues is the essence of the Arnoldi algorithm.

For the case of a real symmetric or complex Hermitian matrix A, severe simplifications can be made, in particular, H becomes tridiagonal. Both computational work and required storage drops significantly. Doing these simplifications leads to the Lanczos algorithm.

For practical purposes, one may be interested in finding not the largest eigenvalues, but some eigenvalues close to some arbitrary value ζ. One then instead solves for the eigenvalues of the matrix $(A - \zeta I)^{-1}$.

In this project, a Lanczos algorithm was used to find approximations to eigenvalues and eigenvectors. In order to be able to handle complex numbers and the so-called *pole approximation*, a custom written[25] algorithm was used rather than a standard one. The pole approximation in essence means that the eigenvector corresponding to both particles in the resonant state without interaction is chosen as a starting vector for the iteration.

The value obtained by the custom written software was unstable, and rather gave a hint of the region in which to find the actual eigenvalue. After that, an Arnoldi method in `ARPACK` (see Appendix E) was used.

Appendix C

Feshbach Resonances

The interaction strength between atoms in the trap, manifested in Equation (3.17), is controllable by changing the external magnetic field applied to the system. This dependence is due to a so-called Feshbach resonance. Here, a brief and somewhat simplified summary is provided. The underlying theory is involved, and is explained more thoroughly in other literature [16, 23].

Consider a low-energy scattering event of two particles in a spherically symmetric relative-particle potential that goes to zero outside some finite radius. A partial-wave expansion can be performed both on the potential and the particle wavefunction, which essentially means expressing them as a sum of spherical harmonics times radial parts. If the energy in a scattering event is low enough, the particle de Broglie wavelength will be too long for it to resolve all the details of the scattering potential. The contribution from the lowest angular momentum state, the so-called s-wave, will then dominate the expansion.

We define a *scattering channel* as a set of quantum numbers. For example, this can be different spin configurations. Consider such a two-particle system consisting of two scattering channels, which we denote as the open channel and the closed channel. The open channel has only scattering states, while the closed channel has a bound state. See Figure C.1. The resonance occurs when the bound state in the closed channel energetically approaches the zero-energy scattering state in the open channel. This leads to strong mixing of the states.

Since the magnetic moment for different spin configurations may differ, the energy levels can be shifted by changing an external magnetic field. Thereby, the energy of the bound state relative to the scattering state can be changed, to bring them closer or further apart. This amounts to changing the inter-particle interaction. It can be shown that the coupling coefficient g in (3.17) is proportional to the inverse of the difference in energy between the bound and resonant states.

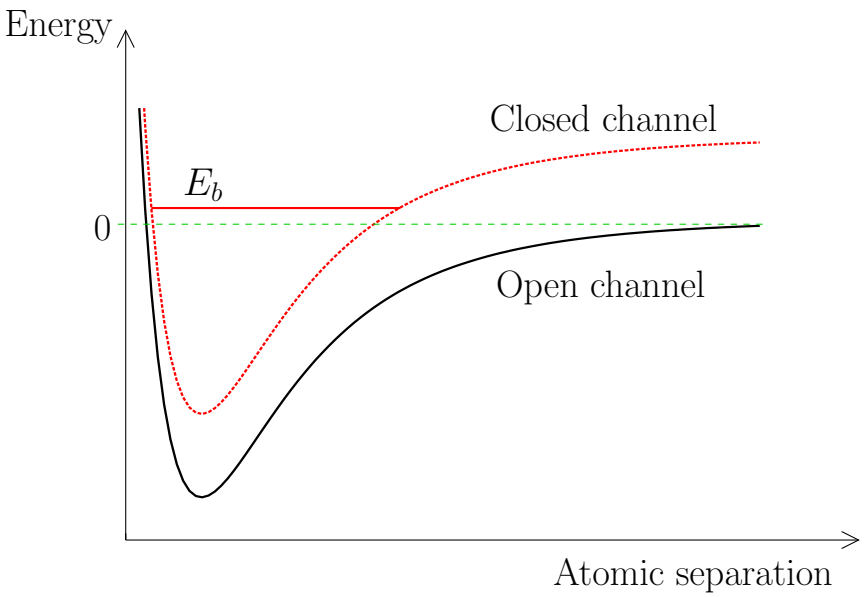

Figure C.1. *Illustration of two potentials corresponding to open and closed channels, respectively. E_b is the energy of the bound state in the closed channel.*

Appendix D

Wentzel–Kramers–Brillouin Approximation

This appendix contains a short overview of the WKB approximation. A more complete coverage, including derivations of relevant equations, is given by for example [24, pp. 315-339].

The time-independent Schrödinger equation in one dimension can be rewritten as

$$\frac{\mathrm{d}^2\psi}{\mathrm{d}x^2} = -\frac{p^2}{\hbar^2}\psi \tag{D.1}$$

with $p(x) = \sqrt{2m\left[E - V(x)\right]}$. Rewriting the wavefunction as its amplitude $A(x)$ times its phase $e^{i\phi(x)}$, where both $A(x)$ and $\phi(x)$ are real, we get $\Psi(x) = A(x)e^{i\phi(x)}$. Inserting this into the Schrödinger equation gives us two equations equivalent to (D.1), one for the real part and one for the imaginary part:

$$\begin{cases} A'' &= A\left[(\phi')^2 - \frac{p^2}{\hbar^2}\right] \\ (A^2\phi')' = 0 \end{cases}$$

Solving the second of these equations yields

$$A = \frac{C}{\sqrt{\phi'}}$$

while the first equation is not in general solvable. One then makes a crucial approximation: The amplitude of A varies slowly, so that $A''/A \ll (\phi')^2$ and $A''/A \ll p^2/\hbar^2$. The A'' term can then be dropped, resulting in the solution

$$\phi(x) = \pm\frac{1}{\hbar}\int p(x)\mathrm{d}x$$

which gives the total wavefunction as

$$\psi(x) = \frac{C}{\sqrt{p(x)}} e^{\pm \frac{i}{\hbar} \int p(x) \mathrm{d}x} \tag{D.2}$$

and the general solution is a linear combination of two of these, with different signs. For the potential in our problem, we can divide it into three regions, as in Figure D.1, where region I and III are *classically allowed* and region II is *classically forbidden*. Region I is the trap region for our particle. Note that $p(x)$ is imaginary in the classically forbidden regions.

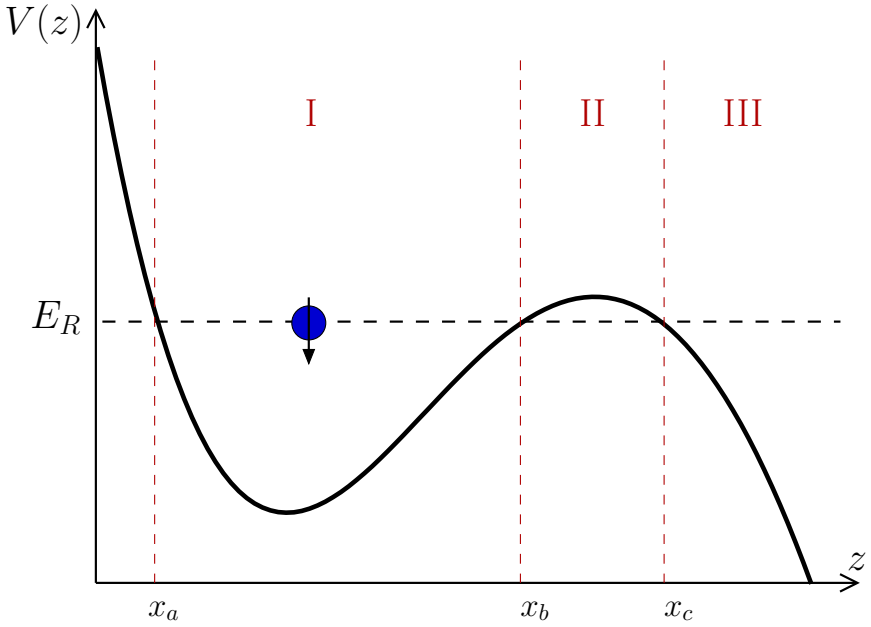

Figure D.1. *Illustration of a trap with a resonant state, partitioned into three different regions. These regions are used in the WKB approximation described in the text.*

This approximation obviously breaks down at the so-called *classical turning points* x_a, x_b and x_c, where $p(x) = 0$. In order to remedy this, the potential is linearized in the vicinity of these points, and the Schrödinger equation is solved for the linearized potential. Thereafter, the equation (D.2) is patched together around the turning point by using the linearized solution, which turns out to be a so-called Airy function. This patching gives rise to conditions on the momentum. For our trap region, this implies that

$$\int_{x_a}^{x_b} \mathrm{d}x p(x) = \left(n - \frac{1}{2}\right) \pi\hbar$$

with n a positive integer, from which one can find the energy levels inside the trap.

If one now looks at transmission through a barrier, assuming a broad and high barrier, only the exponentially decaying solution will be physical. One can then show that the transmission factor is

$$T = e^{-2\xi}$$

where $\xi \equiv \int_{x_b}^{x_c} \mathrm{d}x\, |p(x)|$. Assuming that the particle "bounces" between the walls with a frequency obtained from a harmonic oscillator approximation,

$$\nu = \frac{E}{2\pi\hbar},$$

the probability of tunneling is then $\gamma \equiv \nu f$ for every time unit.

D.1 Validity of the WKB Approximation

Some remarks on the validity of the WKB approximation in our specific potential can be made, using the shape of the wavefunction obtained from a basis expansion. For instance, the assumptions $|A''/A| \ll \left|\phi'^2\right|$ and $|A''/A| \ll \left|p^2/\hbar^2\right|$ may easily be checked. These are shown in Figure D.2, and as can be seen, these assumptions are not even close to fulfilled inside the trap.

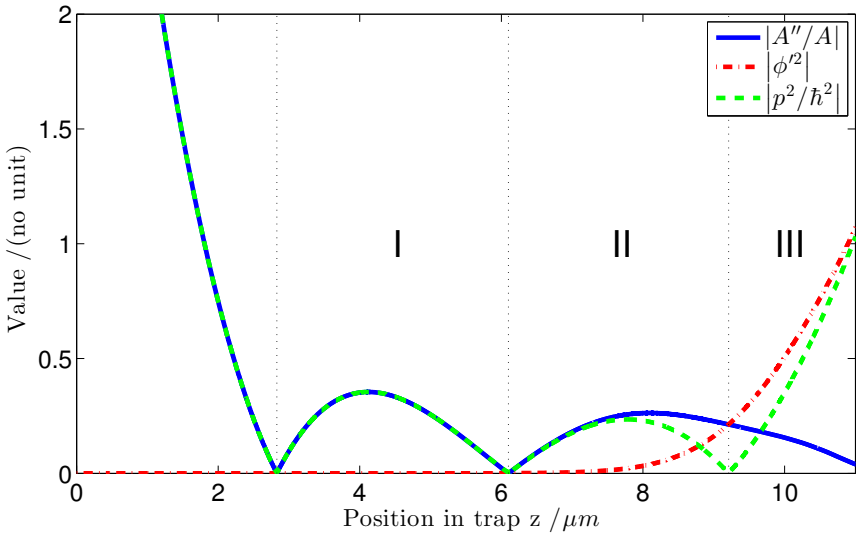

Figure D.2. *Values of three quantities relevant for one of the approximations made in a WKB calculation, as described by the text. The trap is given by* (4.1) *using* $c_{|\uparrow\rangle} = 1.00457$ *and the regions are defined as above.*

Appendix E

Software Libraries

This project has utilized a number of external software libraries, some of which are described below. Note that many of the libraries are available as Debian packages.

Library: LAPACK – Linear Algebra PACKage

Description: Library with linear algebra routines, such as QR iteration for finding eigenvalues.

Download: `http://www.netlib.org/lapack`

License: *Modified BSD, http://www.netlib.org/lapack/LICENSE.txt*

Library: ARPACK – ARnoldi PACKage

Description: Library with the restarted Arnoldi method for finding eigenvalues

Download: `http://www.caam.rice.edu/software/ARPACK/`

License: *Modified BSD, http://www.caam.rice.edu/software/ARPACK/RiceBSD.txt*

Library: BLAS – Basic Linear Algebra Subprograms

Description: Routines that provide standard building blocks for performing basic vector and matrix operations. Used by `LAPACK` and `ARPACK`.

Download: `http://www.netlib.org/blas/`

License: *Modified BSD, http://www.netlib.org/lapack*

Library: Libconfig

Description: Library used to read configuration files.

Download: `http://www.hyperrealm.com/libconfig/`

License: *LGPL, http://www.gnu.org/licenses/lgpl.html*

Library: RLlib

Description: Standard routines for `C++` code.

Download: urlhttps://github.com/riklund/rllib

License: *GPL, http://www.gnu.org/licenses/gpl.html*

Library: Function Parser

Description: Library to parse mathematical expressions.

Download: `http://warp.povusers.org/FunctionParse`

License: *LGPL, http://www.gnu.org/copyleft/lesser.html*

Library: Intel Math Kernel Library

Description: Library containing optimized version of LAPACK.

Download: `http://software.intel.com/en-us/intel-mkl`

License: *Proprietary*